

## Article (refereed) - postprint

---

Rameshwaran, Ponnambalam; Naden, Pamela; Wilson, Catherine A.M.E.; Malki, Rami; Shukla, Deepak R.; Shiono, Koji. 2013. **Inter-comparison and validation of computational fluid dynamics codes in two-stage meandering channel flows.**

© 2013 Published by Elsevier Inc.

This version available <http://nora.nerc.ac.uk/503241/>

NERC has developed NORA to enable users to access research outputs wholly or partially funded by NERC. Copyright and other rights for material on this site are retained by the rights owners. Users should read the terms and conditions of use of this material at <http://nora.nerc.ac.uk/policies.html#access>

NOTICE: this is the author's version of a work that was accepted for publication in *Applied Mathematical Modelling*. Changes resulting from the publishing process, such as peer review, editing, corrections, structural formatting, and other quality control mechanisms may not be reflected in this document. Changes may have been made to this work since it was submitted for publication. A definitive version was subsequently published in *Applied Mathematical Modelling* (2013), 37 (20-21). 8652-8672.

[10.1016/j.apm.2013.07.016](https://doi.org/10.1016/j.apm.2013.07.016)

[www.elsevier.com/](http://www.elsevier.com/)

Contact CEH NORA team at  
[noraceh@ceh.ac.uk](mailto:noraceh@ceh.ac.uk)

# Inter-Comparison and Validation of Computational Fluid Dynamics Codes in Two-stage Meandering Channel Flows

Ponnambalam Rameshwaran<sup>1</sup>, Pamela Naden<sup>1</sup>, Catherine A.M.E.Wilson<sup>2</sup>, Rami Malki<sup>2</sup>, Deepak R Shukla<sup>3</sup> & Koji Shiono<sup>3</sup>

<sup>1</sup>Centre for Ecology and Hydrology, Wallingford, OX10 8BB, UK

<sup>2</sup>Hydro-environmental Research Centre, Cardiff School of Engineering, Cardiff University, Queen's Buildings, Cardiff, CF24 3AA, UK

<sup>3</sup>Department of Civil and Building Engineering, Loughborough University, Loughborough, LE11 3TU, UK

## Abstract

This paper presents a study in the inter-comparison and validation of three-dimensional computational fluid dynamics codes which are currently used in river engineering. Finite volume codes PHOENICS, FLUENT and SSIIM; and finite element code TELEM3D are considered in this study. The work has been carried out by competent hydraulic modellers who are users of the codes and not involved in their development. This paper is therefore written from the perspective of independent practitioners of the techniques. In all codes, the flow calculations are performed by solving the three-dimensional continuity and Reynolds-averaged Navier-Stokes equations with the  $k-\epsilon$  turbulence model. The application of each code was carried out independently and this led to slightly different, but nonetheless valid, models. This is particularly seen in the different boundary conditions which have been applied and which arise in part from differences in the modelling approaches and methodology adopted by the different research groups and in part from the different assumptions and formulations implemented in the different codes. Similar finite volume meshes are used in the simulations with PHOENICS, FLUENT and SSIIM while in TELEM3D, a triangular finite element mesh is used. The ASME Journal of Fluids Engineering editorial policy is taken as a minimum framework for the control of numerical accuracy. In all cases, grid convergence is demonstrated and conventional criteria, such as  $Y^+$ , are satisfied. A rigorous inter-comparison of the codes is performed using large-scale experimental data from the UK Flood Channel Facility for a two-stage meandering channel. This example data set shows complex hydraulic behaviour without the additional complications found in natural rivers. Standardised methods are used to compare each model with the available experimental data. Results

are shown for the streamwise and transverse velocities, secondary flow, turbulent kinetic energy, bed shear stress and free surface elevation. They demonstrate that the models produce similar results overall, although there are some differences in the predicted flow field and greater differences in turbulent kinetic energy and bed shear stress. This study is seen as an essential first step in the inter-comparison of some of the computational fluid dynamics codes used in the field of river engineering.

**Keywords:** Computational Fluid Dynamics (CFD), Floodplain, Hydraulic models, Model uncertainty, River engineering, Two-stage meandering channel

## Introduction

In recent years, three-dimensional (3D) Computational Fluid Dynamics (CFD) codes have been increasingly used in a number of river engineering applications, notably those which need distributed output from a complex flow field. There are a number of general purpose and free-surface flow 3D CFD codes available commercially and academically which can be used in river engineering. They all provide a numerical solution of the continuity and Reynolds-averaged Navier-Stokes (RANS) equations with a turbulence closure model but each code incorporates slightly different assumptions and formulations, offers different options for the numerical solution of the equations and puts different constraints on boundary conditions such as the roughness function. Despite the recent applications of CFD codes in the complex natural environment such as a meander channel, river confluences and flood flows (e.g. Bradbrook *et al.*, [1]; Hodkinson and Ferguson, [2]; Lane *et al.*, [3] and Nicholas and McLelland, [4]; Rameshwaran and Naden [5]), there has been very little effort made in inter-comparison and validation of these codes. Indeed, Rameshwaran and Naden [6] and Wilson *et al.* [7] compared the performance of a 2D depth-averaged code and a 3D code in the numerical simulation of flows in a meandering compound channel however, given the numerous CFD codes available and the importance of river and flood modelling, there is a growing demand for more comparative studies to be conducted.

The objective of this paper is to provide a quantitative evaluation of CFD codes by performing benchmark testing against a complex turbulent flow case. As a first step, this paper uses four of the available CFD codes – PHOENICS, FLUENT, SSIIM and TELEMAC3D. A steady state turbulent flow in a two-stage meandering channel is considered because it produces a more complex three-dimensional flow behaviour, resulting from the interaction between the floodplain flow and the main

channel flow, than that in simple open channels [8, 9]. All simulations were performed by different research groups who are competent hydraulic modellers and users of CFD but not involved in the development of the codes. Although, each group has tried to use a similar modelling approach, this was not always possible because of constraints embedded within each code. The performance of the 3D codes is evaluated by a rigorous comparison of results generated by each group and with the detailed experimental data obtained from the UK Flood Channel Facility (UK-FCF). The simulated results are compared in terms of streamwise transverse velocities, secondary flow, turbulent kinetic energy, bed shear stress and free surface elevation. An overall assessment of model uncertainty is also provided.

The accuracy of a CFD model of the physical system is governed by the numerical technique used to solve the governing equations and the initial and boundary conditions used to specify the problem. In recent years, several journals have adopted an editorial policy statement on numerical accuracy to improve the quality of publications (e.g. American Society of Mechanical Engineers (ASME) Journals and American Institute of Aeronautics and Astronautics (AIAA) Journals [10]). The ASME Journal of Fluids Engineering editorial policy [10] statement is considered as a minimum framework for this model inter-comparison and validation study. For natural open channel flows, Lane *et al.* [11] made some additional comments on these policy statements which are also considered.

### **CFD Codes**

The CFD codes considered in this study are PHOENICS (Version 3.5), FLUENT (Version 6.1), SSIIM (Version 1) and TELEMAC3D (Version V5P4). PHOENICS and FLUENT are commercially available general purpose CFD codes which are developed by Concentration Heat and Momentum Limited (CHAM) and Fluent Inc respectively. SSIIM is an academic code which is developed by Professor. Nils Reidar B. Olsen and is freely available and specifically geared to river channel applications. TELEMAC3D is an open source code for free-surface flow developed by the Laboratoire National d'Hydraulique, Electricité de France (EDF). Although the non-hydrostatic version of TELEMAC3D is used in this study, it does differ from the other codes in that it solves the RANS equations for velocity and depth, rather than velocity and pressure. It is also a finite element code whereas the other three are finite volume codes. Whichever numerical code is used, a suitable mesh has to be chosen and additional assumptions have to be made regarding the boundary conditions, turbulence model and the numerical scheme used to solve the equations.

## Experimental Data

A brief description of the UK Flood Channel Facility Series B experimental set up is given below since the data were used in this investigation. The Series B programme has been described by Ervine *et al.* [8] and Sellin *et al.* [12]. Series B experiments were for the study of meandering channels with non-mobile channel beds (Figure 1). The UK Flood Channel Facility flume is 60 m long and 10 m wide, with a maximum discharge of  $1.1 \text{ m}^3\text{s}^{-1}$ . Experiments were performed in two-stage meandering channels consisting of flat floodplains with straight floodplain walls and a sinuous main channel, as shown in Figure 2 and Table 1. The top width of the main channel was 1.2 m and the bank slopes were  $45^\circ$  with a bank-full depth of 0.15 m (Figure 2b). The sinuosity of the channel was 1.374 and the longitudinal channel slope was  $0.996 \times 10^{-3}$ . The flow rate was measured using calibrated orifice plates. The water surface elevations were measured using digital point gauges. Detailed free-surface elevation and measurements of horizontal velocity were made in a series of cross-sections spaced along the channel under steady flow. The discharge was  $0.25 \text{ m}^3\text{s}^{-1}$  and the water depth in the main channel was 0.2 m. The flow angle was recorded by a vane connected to a rotary potentiometer and the horizontal velocity was measured using a miniature propeller meter. In addition, at the main channel apex cross-section, turbulence measurements were undertaken using a two-component Laser Doppler Anemometer (LDA) system and the bed shear stress was measured by a Preston tube on the bed. In ideal flow conditions, the stated accuracy of the instrumentation is as follows: orifice plate  $\pm 2\%$ , digital point gauge  $\pm 0.05 \text{ mm}$ , vane with rotary potentiometer  $\pm 0.5\%$ , miniature propeller meter  $\pm 1\%$ , LDA  $\pm 0.2\%$  and Preston tube  $\pm 0.25\%$ .

## Hydrodynamic Model Equations

The governing equations for open channel flow are the continuity and Reynolds-averaged Navier-Stokes (RANS) equations. For incompressible flow, the continuity and momentum equations can be written in Cartesian coordinates as:

$$\partial U_i / \partial x_i = 0 \quad (1)$$

$$\partial U_i / \partial t + U_j \partial U_i / \partial x_j = -(1/\rho) \partial P / \partial x_i + \partial / \partial x_j [ \nu (\partial U_i / \partial x_j + \partial U_j / \partial x_i) - \overline{u'_i u'_j} ] + g_i \quad (2)$$

where  $i$  and  $j$  are standard tensor notation indicating two out of the three  $x$ ,  $y$  and  $z$  coordinate directions,  $U_i$  is the time-averaged velocity component in  $x_i$  direction,  $u'_i$  is the fluctuating part of the velocity in  $x_i$  direction,  $\rho$  is the density,  $P$  is the pressure,  $g_i$  is the gravity force per unit volume and  $\nu$

is the kinematic viscosity. The turbulent Reynolds stresses  $-\overline{u'_i u'_j}$  are calculated with the standard  $k$ - $\varepsilon$  turbulence model [13]:

$$-\overline{u'_i u'_j} = \nu_t (\partial U_i / \partial x_j + \partial U_j / \partial x_i) - (2/3) k \delta_{ij} \quad (3)$$

where  $k$  is the turbulent kinetic energy,  $\delta_{ij}$  is the Kronecker delta function and  $\nu_t$  is the turbulent eddy viscosity. The turbulent eddy viscosity is expressed in terms of the turbulent kinetic energy  $k$  and the turbulent kinetic energy dissipation  $\varepsilon$  via the Kolmogorov-Prandtl expression:

$$\nu_t = c_\mu k^2 / \varepsilon \quad (4)$$

where  $c_\mu$  is a constant. The turbulent kinetic energy  $k$  and dissipation of turbulent kinetic energy  $\varepsilon$  quantities are determined from the transport equations:

$$\partial k / \partial t + U_i \partial k / \partial x_i = \partial / \partial x_i [(v_t / \sigma_k) \partial k / \partial x_i] + P_k - \varepsilon \quad (5)$$

$$\partial \varepsilon / \partial t + U_i \partial \varepsilon / \partial x_i = \partial / \partial x_i [(v_t / \sigma_\varepsilon) \partial \varepsilon / \partial x_i] + \varepsilon / k (c_{1\varepsilon} P_k - c_{2\varepsilon} \varepsilon) \quad (6)$$

where  $\sigma_k$ ,  $\sigma_\varepsilon$ ,  $c_{1\varepsilon}$ , and  $c_{2\varepsilon}$  are empirical constants and  $P_k$  is the production of turbulent energy  $k$  defined as:

$$P_k = \nu_t (\partial U_i / \partial x_j + \partial U_j / \partial x_i) \partial U_i / \partial x_j \quad (7)$$

The standard values of the model constants are  $c_\mu = 0.09$ ,  $c_{1\varepsilon} = 1.44$ ,  $c_{2\varepsilon} = 1.92$ ,  $\sigma_k = 1.0$  and  $\sigma_\varepsilon = 1.3$ .

In PHOENICS, FLUENT and SSIIM codes, the 3D flow calculations were performed by solving the RANS equations with the  $k$ - $\varepsilon$  turbulence model for steady-state flow where the time-dependent terms in equations (2), (5) and (6) are zero. In TELEMACH3D, the transient flow equations were solved until a steady-state flow condition is reached.

## Boundary Conditions

There are four different types of boundaries that are distinguished in this two-stage meandering channel test case namely inlet, outlet, bottom boundary and water surface boundary. The boundary conditions used are as follows and summarised in Table 2.

### Inlet

In all codes, the boundary condition for the inlet is the mean streamwise velocity and other variables are set to zero. Refinements to this are that, in SSIIM, the initial run uses a logarithmic profile of velocities scaled to give the correct discharge, and in PHOENICS, SSIIM and FLUENT after the initial model run, fully developed flow conditions are used for the inlet boundary condition.

### **Outlet**

At the outlet, PHOENICS, FLUENT and SSIIM use the boundary condition of zero pressure on the free surface and TELEM3D uses the measured water elevation. In all codes, the zero normal derivatives of velocity, turbulent kinetic energy and energy dissipation rate are set internally at the outlet plane (i.e.  $\partial U_i / \partial m = \partial k / \partial m = \partial \varepsilon / \partial m = 0$  where  $m$  is the direction normal to the outlet plane).

### **Bottom channel boundary**

In all codes, the bottom channel boundary condition is defined using a standard wall-function to describe the fully turbulent region outside the viscous sub-layer [14]:

$$U_\tau / U_* = (1/\kappa) \ln(EY^+) \quad (8)$$

$$\text{with } U_* = (\tau_b / \rho)^{0.5}; \quad Y^+ = U_* Y / \nu \quad (9)$$

where  $U_\tau$  is the resultant velocity parallel to the wall at the first cell,  $U_*$  is the resultant friction velocity,  $\kappa$  is the von Karman constant equal to 0.41,  $Y^+$  is the non-dimensional wall distance,  $\tau_b$  is the bed shear stress,  $Y$  is the normal distance to the wall and  $E$  is a roughness parameter function. The differences between the roughness parameter function  $E$  used in each of the codes are shown in Table 3. Within SSIIM and TELEM3D, only the fully rough law has been implemented whereas both PHOENICS and FLUENT include formulations for hydraulically smooth, transitional and fully rough boundaries. The near wall values of turbulent kinetic energy  $k$  and dissipation  $\varepsilon$  are also specified by assuming local equilibrium of turbulence in all codes [13]:

$$k = U_*^2 / c_\mu^{0.5}; \quad \varepsilon = U_*^3 / (\kappa Y) \quad (10)$$

### **Water surface boundary**

In TELEM3D, the conservative form of the free surface equation is used to calculate the water surface elevation which is written as [15]:

$$\partial S / \partial t + \partial / \partial x \int_{-z}^S U dz + \partial / \partial y \int_{-z}^S V dz = 0 \quad (11)$$

where  $S(x,y,t)$  is the free-surface elevation and  $Z(x,y)$  is the bed elevation. In the other codes, PHOENICS, FLUENT and SSIIM, the water surface needs to be defined in the model mesh (i.e. fixed lid approach). At the water surface, the velocity normal to the surface and the normal gradients of other velocity components, turbulent kinetic energy and energy dissipation rate are set to zero in all codes. In PHOENICS, a free surface treatment for the spatial variation of the water surface is adopted where the fixed lid is adjusted iteratively until the pressure at the free surface reduces to zero. The detail of the

procedure is given in Rameshwaran and Naden [5]. There is potential to use a non-fixed lid approach with simulations using both FLUENT and SSIIM but this was not taken up.

## Meshes

Meshes were built for two meandering channel wavelengths for this study. In PHOENICS, FLUENT and SSIIM, body fitted co-ordinates are used in the Cartesian frame to generate nearly identical meshes for model comparison based on the assumption that the water surface is planar. TELEMAC3D uses a two-dimensional (2D) mesh as a base mesh to generate the full 3D mesh. The 2D mesh is an unstructured triangular finite element mesh based on Delaunay triangulation. The 3D mesh is then obtained by duplicating the 2D base mesh over layers along the vertical. For the economy of the solution and computational time, only 18 horizontal layers were used in TELEMAC3D mesh compared to other meshes where 20 cells were used in vertical plane. The details of the meshes are tabulated in Table 4. In all cases, a fine mesh was used in the main channel whereas a coarser mesh was used on the floodplain. Figure 3 shows the top plan and apex cross-sectional views of the meshes. In all cases, the best practice guideline of ensuring that  $Y^+$  is between 30 and 130 (i.e. within the fully turbulent region) at almost all points on the boundary was met.

Additional meshes were generated and model runs were also undertaken to ensure that grid convergent solutions were being considered. This was done by running three versions of each model with successively coarser meshes as suggested by Roache [16] and examining the change in correlation between model results as described in Hardy *et al.* [17] and Rameshwaran and Naden [5].

## Numerical Algorithm and Solution Techniques

The PHOENICS, SSIIM and FLUENT finite volume codes solve the governing partial differential equations (1), (2), (5) and (6) for steady-state flow. These conservation equations can be written in the same general differential form:

$$\partial/\partial x_i(\rho U_i \phi - \Gamma_\phi \partial \phi / \partial x_i) = S_\phi \quad (12)$$

where  $\phi$  is the variable depending on the equation considered,  $\Gamma_\phi$  is the diffusion coefficient of the variable  $\phi$ , and  $S_\phi$  is the source term in the equation. The discretised equations are obtained by integrating equation (12) over each computational cell. A non-staggered approach was used to solve the

equations in the PHOENICS, SSIIM and FLUENT codes. The pressure-velocity coupling is achieved using the SIMPLEC algorithm [18] in PHOENICS and SIMPLE algorithm [19] in both SSIIM and FLUENT. The approximation of the convection term is handled by the QUICK-based non-linear higher order scheme SMART [20] in PHOENICS and second order upwind scheme in both SSIIM and FLUENT. These methods comply with best practice guidelines for CFD (e.g. ASMA). The discretised equations are solved with a Stone-based extension of a tri-diagonal solver in PHOENICS, Gauss-Seidel solver with a Multi-block convergence acceleration algorithm in SSIIM and the implicit solver in FLUENT.

In TELEMAC3D, a finite element discretisation is employed to solve the transient flow equations (1), (2), (5) and (6) along with the conservative form of the free surface equation (11). The algorithm is based on a fractional step technique in which the governing equations are split into fractional steps and treated using appropriate numerical schemes for the advection of flow variables. The semi-implicit Streamline Upwind Petrov–Galerkin (SUPG) scheme [21] is used for the advection of velocities and water depth. The method of characteristics [22] is used for the advection of  $k$  and  $\varepsilon$ . The semi-implicit standard Galerkin finite element method is used to solve the diffusive terms of the governing momentum equations. The conservative free-surface equation is solved using the semi-implicit SUPG scheme. The linearised system of equations is solved by an iterative method with an accuracy of  $10^{-6}$ . A detailed description of the solution algorithm of the non-hydrostatic TELEMAC3D code is provided by Jankowski [15] and Hervouet and Jankowski [23].

In all codes, computation starts from quiescent initial conditions with appropriate boundary conditions. In subsequent runs, the convergence procedure is accelerated by adopting prior steady state solutions as initial conditions. Mass balance, residual and/or flow value behaviour for each solved variable are used to detect convergence to a steady state. The criteria for convergence in the PHOENICS, SSIIM and FLUENT codes are that the residuals are reduced to 0.1%, the mass balance is within 0.1% and the flow values have settled down to an almost constant value. In TELEMAC3D, the solution is assumed to have converged and reached steady state when the mass is balanced within 1% and the absolute incremental values of the flow variables between the two time steps at all the nodes are less than  $10^{-4}$ . Table 5 summaries the solution techniques in all codes.

## Model Results and Discussion

In the following presentation of the results, PHOENICS, SSIIM, FLUENT and TELEMAC3D are used to describe the simulations. As explained above, these terms refer to the complete model (i.e. code plus mesh, assumptions and calibration) rather than solely to the numerical code. In the figures which relate to the channel, the direction along the meandering main channel wall was defined as the streamwise coordinate  $x$  and that perpendicular to  $x$  as the lateral coordinate  $y$  (Figure 2 – Cross-sections MC1 to MC11). Ordinary Cartesian coordinates were used for the floodplain in which the longitudinal direction parallel to the straight flood bank was defined as the coordinate  $x$  and that perpendicular to  $x$  as the coordinate  $y$  (Figure 2 – Cross-sections FP1 to FP9). In order to compare the results from any particular model both with the available data and with the other models, the results were interpolated to the location of the data points, using the same kriging technique. In the scatter plots, all the possible pairwise comparisons for the flow variables throughout the main channel from cross sections MC1 to MC11 and on the floodplain cross-sections FP1 to FP9 are shown with the 1:1 agreement line and linear regression line fitted by least squares. The regression coefficients are tabled below the plots. Plotting each of the individual graphs both ways round provides forwards and backwards regression lines, based on minimising the errors in each variable separately (cf. [24]). The degree of scatter is indicated by the coefficient of determination ( $R^2$ ), while the slope ( $m$ ) and intercept ( $c$ ) indicate any bias in the pairwise comparison.

### *Model calibration and Roughness*

Once the models were set up by specifying appropriate boundary conditions as input data and an initial run performed until they converged, either the pressure distribution at the free surface in the cases of PHOENICS, SSIIM and FLUENT, or the water depth in the case of TELEMAC3D, was examined and the roughness parameter  $k_s$  adjusted until the modelled water surface matched the measured longitudinal gradient. Variations between the formulations of the bottom boundary roughness function (Table 3) and solution techniques (Table 5) mean that each model takes a slightly different value of  $k_s$  as shown in Table 6. The boundary roughness function dependence on the roughness Reynolds number (Table 3) means that both PHOENICS and FLUENT use the transitional equation in nearly all flow areas both in the main channel and on the floodplain, but both SSIIM and TELEMAC3D only have the option of the fully rough version of the roughness function. Different solution techniques produce different degrees of numerical diffusion within model. The numerical diffusion acts as artificial friction

within the model, hence the smaller the numerical diffusion the higher the calibrated roughness parameter  $k_s$  [25]. This may be the case for PHOENICS where the use of the higher order numerical scheme (Table 5) resulted in the highest value for the roughness parameter  $k_s$ . On other hand, it is also well know that the strength of the turbulence field and secondary circulations are not adequately modelled with the  $k$ - $\epsilon$  turbulence model and a higher roughness parameter is needed to counteract this and achieve the momentum balance indicated by the experimental measurements [5]. The roughness parameter can also compensate for a coarse grid resolution [26] and this issue is addressed in the following section. In the experiment, channel surfaces were made of smooth cement mortar. The skin friction of the channel surface, as measured in a calibration experiment, was approximately 0.3 mm [5]. However, Table 6 shows that the specified roughness values for PHOENICS and TELEMAC3D models are slightly higher than the experimentally calculated skin friction and for the SSIIM and FLUENT models are slightly less. This shows that calibrated roughness values can be dependent on several factors within the model set up.

### ***Grid independence tests***

The effects of grid dimensions were examined by comparing results across three different size meshes as described by Roache [16]. The grid refinement ratio, in all directions, between the coarsest and finest meshes (M1 to M3) is 2.0 i.e. the number of cells in all directions was doubled. Ratios for intermediate meshes are 1.50 for M1-M2 and 1.33 for M2-M3. Details of the M3 mesh are given in Table 4. The quantitative comparison of the streamwise velocity, transverse velocity, turbulent kinetic energy and bed shear stress are shown in Figure 4 for the PHOENICS model runs. Similar results were found for the other models investigated but, for brevity, only the PHOENICS model results are shown here as an example. The comparisons are made based on the lower resolution mesh points with the results from the higher resolution mesh interpolated onto lower resolution mesh points. Figure 4 shows that both the slope and intercept of the regression lines tend towards 1 and 0 respectively and the correlation values improve as the mesh is refined. Figure 4 also shows that the M2-M3 results are in good agreement, with a correlation value of 1.0 for streamwise velocity, transverse velocity and turbulent kinetic energy and 0.99 for bed shear stress. M1-M2 and M1-M3 results are slightly more scattered particularly for turbulent kinetic energy and bed shear stress which are most sensitive to mesh resolution as noted in other studies [17, 24]. The calculations of the median values of the Grid Convergence Index (GCI) based on Roache [16] in Table 7 for the streamwise velocity, transverse velocity, turbulent kinetic energy and bed shear stress suggest that the predictions have converged

towards a mesh independent solution, indicating that the finer mesh used in this study provides solutions which are relatively free of numerical error.

### ***Streamwise velocity***

Figures 5 and 6 show the scatter plot comparisons for the streamwise velocity in the main channel and on the floodplain respectively. Although there is considerable scatter in the plots, there is a similar level of agreement between all the models and the available data. It is also clear from regression coefficients in Figures 5 and 6 that the models perform much better in the main channel than on the floodplain, where all the models show considerable scatter and a tendency to overpredict the higher streamwise velocities and underpredict the lower streamwise velocities. On the floodplain, it is also clear from Figure 6 that the model results fall into two pairs with PHOENICS and TELEMAC3D behaving in a similar fashion and SSIIM and FLUENT showing close agreement. Looking at the results in detail, both SSIIM and FLUENT tend to give higher streamwise velocity on either side of the floodplain outside the meandering belt and lower streamwise velocity within the meandering belt compared to PHOENICS and TELEMAC3D. SSIIM predictions are more pronounced in this regard than FLUENT predictions. Figure 7 compares the contour plots of the measured and predicted streamwise velocity distributions at the main channel apex cross-section MC3 and a cross-over section MC8. It shows that TELEMAC3D is slightly better at predicting the maximum flow regions, while FLUENT underpredicts the maximum flow regions in comparison with other models. Figures 5 and 7 also show that the streamwise velocity in the main channel is slightly underpredicted by all models. This may be due to some discrepancy between the methods of measurement where the discharge used to drive the models was measured using an orifice plate meter [6].

### ***Transverse velocity***

Figures 8 and 9 show the scatter plot comparisons for the transverse velocity in the main channel and on the floodplain respectively. Figure 8 shows that all the models perform in a similar fashion and slightly underestimate the strength (magnitude) of the observed transverse velocity in the main channel. On the floodplain, Figure 9 shows that all the model predictions are more scattered compared to the main channel predictions in Figure 8. It is clear from Figure 9 that PHOENICS performs slightly better in comparison with the data. TELEMAC3D also performs reasonably well against the data, although it shows more scatter. It is also clear from Figures 8 and 9 that the models perform better in the prediction of the transverse velocity in the main channel than on the floodplain as was the case with the streamwise velocity predictions. Figure 9 also shows that SSIIM and FLUENT tend to overestimate the transverse velocity magnitude on the floodplain. For SSIIM, this is true throughout the flow field

whereas for FLUENT it occurs mainly in the region just beyond the apex of the bend (FP1 to FP3) and in the cross-over region (FP8 and FP9).

### *Secondary flow vectors*

Figure 10 compares the measured and predicted secondary flow vectors at the main channel apex cross-section MC3. It shows that all the models are able to capture both the large clockwise rotating secondary circulation moving toward the inner bank near the free surface and to the outer bank near the bed, and the smaller and weaker secondary circulation near the main channel outer bank region which, near the bed, rotates in the anti-clockwise direction as measured in experiment. Overall, the secondary flow patterns are reasonably well predicted but their strengths are underpredicted as was noted above in relation to Figure 8 (i.e. the magnitude of the secondary flow vectors). This is a common finding for the standard  $k-\epsilon$  and similar isotropic turbulence models which tend to underpredict the secondary flow strength [6, 27, 28].

### *Turbulent kinetic energy (TKE)*

Figures 11 and 12 show the scatter plot comparisons of the turbulent kinetic energy from the models for the main channel and floodplain respectively. Measured turbulent kinetic energy is only available for the apex main channel cross-section. Figure 11 shows that there is substantial agreement between PHOENICS and SSIIM with both limited scatter and little bias in the main channel. Compared to these models, FLUENT and, more particularly, TELEMAC3D tend to show greater scatter and a substantial bias. In Figure 12, SSIIM and FLUENT show close agreement in the turbulent kinetic energy prediction on the floodplain while PHOENICS and TELEMAC3D tend to predict higher and lower values respectively. Looking more closely at the data, it is clear that the higher and lower values predicted by PHOENICS and TELEMAC3D mainly arise in the cross-over region of the floodplain downstream of the main channel apex between FP5 and FP9 where the flow is expelled from the main channel onto the floodplain. In the comparison of PHOENICS with FLUENT/SSIIM, it is these high values which are responsible for the apparent systematic difference in the results. FLUENT/SSIIM both used a fixed lid while PHOENICS was run with a free surface treatment which accommodated local variations in the water surface. Comparing the PHOENICS results with those of a PHOENICS run with a fixed lid, it is clear that the high values in this area of the model domain come from the relaxation of the fixed-lid assumption. In general, the data also shows that PHOENICS tends to predict higher values within the meander belt while SSIIM tends to predict higher values on either side of the floodplain

outside the meander belt. On the other hand, FLUENT and TELEMAC3D tend to give lower values on the floodplain from FP1 to FP4 and FP5 to FP9 respectively.

Another way of looking at the turbulence characteristics of the model is through the turbulent eddy viscosity which is a function of both the turbulent kinetic energy and the dissipation of turbulent kinetic energy (Equation (4) above). Comparison of the turbulent eddy viscosity yields much greater agreement between the models developed using the PHOENICS, SSIIM and FLUENT codes than is found for TKE. This follows as the turbulent eddy viscosity represents the balance between turbulent kinetic energy generation and its dissipation. Turbulent eddy viscosity in the model developed using the TELEMAC3D code, by contrast, shows a much large scatter and considerable bias compared to the other models, with low values being calculated for a large number of points where high turbulent eddy viscosity is calculated in the other models. This is evident in both the main channel and the floodplain. It implies that the generation of turbulent kinetic energy is not balanced by its dissipation in the same way as in the other models. This thought to arise from the numerical scheme used in the finite element code of TELEMAC3D compared to the other finite volume codes.

A comparison of turbulent kinetic energy at the main channel apex cross-section MC3 is shown in Figure 13a. It shows that the models behave in a similar way and reproduce the turbulent kinetic energy pattern fairly well but generally underestimate turbulent kinetic energy as expected due to inadequacies in the standard  $k-\varepsilon$  model. SSIIM performs slightly better in predicting the maximum turbulent kinetic energy region at the apex section. At the cross-over section MC8, Figure 13b shows that PHOENICS and SSIIM give higher turbulent kinetic energy than FLUENT and TELEMAC3D across the full width of the channel. It is also clear from data that PHOENICS and SSIIM tend to predict higher values of turbulent kinetic energy throughout the main channel particularly in the cross-over region between cross-sections MC6 to MC11. The underprediction of turbulent kinetic energy in TELEMAC3D may be due to the numerical scheme; the method of characteristics used to solve the advection of  $k$  and  $\varepsilon$  is known to produce some numerical diffusion [25, 29].

### ***Bed shear stress***

A comparison of bed shear stress at the apex of the meander bend is given in Figure 14. This shows that all the models give reasonably good agreement in the main channel. Looking more closely, PHOENICS provides a good simulation of the bed shear stress across the channel including the peak in bed shear stress on the inner bank. This feature is also captured by TELEMAC3D but this model tends

to slightly overestimate the bed shear stress across most of the main channel and to underestimate bed shear stress at the outer bank. Conversely, SSIIM and FLUENT show good agreement with the bed shear stress throughout the outer portion of the main channel but fail to capture the high bed shear stress on the inner bank. On the floodplain, there is a great deal of variation. On the outside of the meander bend, SSIIM provides a good fit to the data whereas all the other models underestimate the bed shear stress. On the rest of the floodplain, SSIIM tends to underestimate the shear stress within the meander belt; FLUENT underestimates the shear stress across the whole width of the floodplain; PHOENICS tend to overestimate the shear stress in some parts of the floodplain within the meander belt while TELEMAC3D provides a reasonably good fit to the data. As expected, the near-bed turbulent kinetic energy behaviour within the models is reflected in the bed shear stress predictions ( $\tau_b = \rho k (c_\mu)^{0.5}$ ).

### ***Free surface elevation***

Finally, a scatter plot comparison of free surface variation along the half wavelength channel is given in Figure 15 for PHOENICS and TELEMAC3D. It can be seen from the figure that the free surface treatment in PHOENICS and model prediction in TELEMAC3D reasonably capture the water surface variation (about  $\pm 4$  mm from mean elevation) arising from the complex three-dimensional flow behaviour generated by the interaction between the floodplain flow and the main channel flow [8]. It is clear from the regression coefficient in Figure 15 that PHOENICS performs slightly better in comparison with the data while TELEMAC3D shows slightly more scatter. Rameshwaran and Naden [5] showed that the representation of the free surface variation in the model is vital for the accurate prediction of bed shear stress. This is due to the fact that if the free surface is modelled (either directly as in TELEMAC3D or through a free-surface treatment as used with PHOENICS), the rate of change of momentum within the water column balances the bed shear stress as in the experimental situation, whereas in the fixed-lid simulation, it has to balance both the bed shear stress and the pressure on the fixed lid. This study demonstrates, as shown in Figure 14 that the bed shear stress is slightly better predicted by PHOENICS and TELEMAC3D than the SSIIM and FLUENT models where the fixed lid approaches were adopted. A comparative model run using the PHOENICS code with a fixed-lid approach showed that the velocity, turbulent kinetic energy and bed shear stress predictions can diverge from the results with the free-surface treatment by up to 6%, 40% and 19% respectively in some areas of the model domain. However, the percentage differences between the PHOENICS fixed-lid model runs versus the SSIIM/FLUENT model runs, and the percentage differences between the PHOENICS free-surface model runs versus the SSIIM/FLUENT model runs indicates that the free surface treatment

used in PHOENICS is only responsible for a relatively small proportion of the difference between the model predictions, except in specific areas of the domain (see above).

### ***Overall assessment***

A comparison of the performance of the individual models has been presented above. This has highlighted differences as well as bringing out the similarities between model performance. As stated earlier, all four simulations are, in practical terms, valid models and another way of looking at the results overall is through an assessment of model uncertainty – both *per se* and in relation to the measured data. This asks the question – how accurate do we expect the results from any valid model? As only four models are compared in this paper, our answer to this question is limited but nonetheless revealing. The first measure of model uncertainty considered is the range of model predictions. For each data point, the range has been calculated by taking the maximum predicted value from any model and subtracting the minimum predicted value from any model. So that the performance across the different variables may be more easily compared, this range has then been normalised by the 90% variation (i.e. 95<sup>th</sup> percentile minus 5<sup>th</sup> percentile) in the variable of interest, taken across all data points, and expressed as a percentage. The 90% variation was used in preference to the absolute range, after looking at the data distributions, in order to avoid influence by outliers. For the velocity variables where data are available across the full flow field, it is the 90% variation in the data which is used. This was found to be very similar to the 90% variation in predictions taken across all models. In the case of the turbulent kinetic energy and the bed shear stress, where the only data available are for the apex cross-section, the 90% variation across all the model predictions was used for normalisation as this provides a better reflection of the whole flow field. This normalised range in model predictions is shown in Figure 16 by both frequency and cumulative percentage distributions for each of the main variables of interest: streamwise and transverse velocity, turbulent kinetic energy and bed shear stress for both the main channel and the flood plain. With the exception of the bed shear stress, there are 1606 points for comparison in the main channel and 544 points on the flood plain. Figure 16 graphically illustrates the large uncertainty between the models for the majority of the variables. The models perform most effectively for the velocities within the main channel and for the turbulent kinetic energy on the flood plain. For these variables, the model uncertainty for more than 85% data points is less than a quarter of the 90% variation in the whole field. What this means in terms of absolute values may be calculated from the table below Figure 16. It shows that, for the main channel velocity, 32% points have a model uncertainty less than  $0.02 \text{ ms}^{-1}$ , while 87% points have a model uncertainty less than  $0.05 \text{ ms}^{-1}$ . On the flood plain, the model uncertainty is much higher; only 39% points have a model

uncertainty for the streamwise velocity less than  $0.06 \text{ ms}^{-1}$  and the majority of points have an uncertainty between 50 and 70% of the 90% variation in the whole field. Compared to measurement uncertainties (see above), these uncertainties are huge. For example, taking the streamwise velocity in the main channel, the instrument uncertainty in the propeller flow meter at the maximum velocity of  $5 \text{ ms}^{-1}$  (i.e. the worst case) is only  $\pm 0.005 \text{ ms}^{-1}$ . Although this does not take into account errors in location or alignment, the model uncertainty in 13% measured points is greater than  $\pm 0.05 \text{ ms}^{-1}$  i.e. a factor ten times the instrument uncertainty.

Where data are available, it is also important to think about the deviation of the models from the data. So Figure 17 provides an equivalent plot of the frequency and cumulative frequency distributions for model error which has been calculated as the absolute maximum deviation from the data taken across all models for each measured point. The plots for the turbulent kinetic energy and the bed shear stress are for the apex section only so the comparison is over a much smaller number of data points as indicated in the table below Figure 17. In all cases, the maximum deviation has been normalised by the 90% variation in the measured data field for each variable and expressed as a percentage. While Figure 17 is broadly similar to Figure 16, it shows that in general, the distributions are shifted to the right indicating that model errors are greater than model uncertainty. This is particularly so for the streamwise velocity within the main channel and possible reasons for this bias were discussed earlier. Interestingly, the model errors for the streamwise velocity on the floodplain are less than the model uncertainty. The poor performance of the models in terms of the turbulent kinetic energy in both the main channel and the flood plain and the bed shear stress on the flood plain for the apex section are clearly shown. However, the bed shear stress in the main channel at the apex section is reasonably well predicted.

## Conclusions

This paper presents an inter-comparison and validation study of four three-dimensional computational fluid dynamics codes – namely, PHOENICS, SSIIM, FLUENT and TELEMAC3D. In all codes, the three-dimensional continuity and Reynolds-averaged Navier-Stokes equations are solved with the standard  $k-\varepsilon$  turbulence model. The performances of the codes are assessed using the experimental data for a two-stage meandering channel obtained from the UK Flood Channel Facility. The criteria outlined in ASME Journal of Fluids Engineering editorial policy [10] on the control of numerical accuracy are met as a minimum framework for this study. The paper demonstrates both the degree of similarity between the model results – providing confidence in the use of these codes – and some of the

differences. The differences are thought to arise from the calibrated roughness values which in turn arise from variations in the model formulations, solution techniques and bottom boundary roughness formulation. In all cases, the streamwise and transverse velocities and secondary flow vectors are reproduced fairly well but there are some differences in turbulent kinetic energy and bed shear stress predictions. In general, predictions for the main channel are better than those for the floodplain. The spatial variation of the water surface is also predicted reasonably well with PHOENICS (with free-surface treatment) and TELEMAC3D. More detailed investigation of the causes of the variation in model results is needed. The exercise presented here is simply seen as a first step in the inter-comparison of available codes; other issues will no doubt arise in model applications to real channels, natural channel boundaries and channels with instream vegetation.

### Acknowledgements

The authors would like to thank all those involved in the UK-FCF programmes for providing the experimental data. Rami Malki acknowledges financial support from EPSRC and Deepak R Shukla acknowledges financial support from the Department of Civil and Building Engineering of the Loughborough University.

### References

- [1] Bradbrook, K.F., Lane, S.N., Richards, K.S., Numerical simulation of time-averaged flow structure at river channel confluences. *Water Resources Research*, **36**, 2731-2746, 2000.
- [2] Hodkinson, A and Ferguson, R.I., Numerical modelling of separated flow in river bends: Model testing and experimental investigation of geometric controls on the extent of flow separation at the concave bank. *Hydrological Processes*, **12**, 1323-1338, 1998.
- [3] Lane, S.N., Bradbrook, K.F., Richards, K.S., Biron, P.A. and Roy, A.G., The application of computational fluid dynamics to natural river channel: three-dimensional versus two-dimensional approaches. *Geomorphology*, **29**, 1-20, 1999.
- [4] Nicholas, A.P. and McLelland, S.J., Computational Fluid Dynamics modelling of three-dimensional processes on natural floodplains. *Journal of Hydraulic Research*, **42**, 131-143, 2004.
- [5] Rameshwaran, P. and Naden, P.S., Three-dimensional modelling of free-surface variation in a meandering channel. *Journal of Hydraulic Research*, **42**, 603-615, 2004.

- [6] Rameshwaran, P. and Naden, P.S., Modelling of turbulent flow in two-stage meandering channels. *Proceedings of the Institution of Civil Engineers-Water Management*, **157**, 159-173, 2004.
- [7] Wilson C.A.M.E., Stoesser T., Olsen N. R. B., Bates P. D., Application and Validation of Numerical Codes in the Prediction of Compound Channel Flows. *Proceedings of the Institution of Civil Engineers, Water, Maritime and Energy*, **153**: 117-128, 2003.
- [8] Ervine, D.A., Willetts, B.B., Sellin, R.H.J. and Lorena, M., Factors affecting conveyance in meandering compound flows. *Journal of Hydraulic Engineering*, **119**, 1383-1399, 1993.
- [9] Shiono, K. and Muto, Y., Complex flow mechanisms in compound meandering channels with overbank flow. *Journal of Fluid Mechanics*, **376**, 221-261, 1998.
- [10] ASME, Journal of Fluids Engineering editorial policy statement on the control of numerical accuracy, *ASME Journal of Fluids Engineering*, **115**, 399, 1993.
- [11] Lane, S.N., Hardy, R.J., Ferguson, R.I. and Parsons, D.R., A framework for model verification and validation of CFD schemes in natural open channel flows. *Computational Fluid Dynamics Applications in Environmental Hydraulics*. Edited by P.D. Bates, S.N. Lane, and R.I. Ferguson, John Wiley and Sons. 169-192, 2005.
- [12] Sellin, R.H.J., Ervine, D.A. and Willetts, B.B., Behaviour of meandering two-stage channels. *Proceedings of the Institution of Civil Engineers - Water Maritime and Energy*, **101**, 99-111, 1993.
- [13] Rodi, W., *Turbulence models and their application in hydraulics*. A.A. Balkema, Rotterdam, 104 pp, 1993.
- [14] Launder, B. E. and Spalding, D. B., The numerical computation of turbulent flows. *Computer Methods in Applied Mechanics and Engineering*, **3**, 269-289, 1974.
- [15] Jankowski, J. A., *Non-hydrostatic model for free surface flows*. PhD thesis, University of Hanover. 237 pp, 1998.
- [16] Roache, P.J., Perspective: A method for uniform reporting of grid refinement studies. *Journal of Fluids Engineering*. **116**, 405-413, 1994.
- [17] Hardy, R.J., Lane, S.N., Ferguson, R.I., and Parsons, D.R. Assessing the credibility of a series of computational fluid dynamic simulations of open channel flow. *Hydrological Processes*, **17**, 1539-1560, 2003.
- [18] Spalding, D.B., Mathematical modelling of fluid mechanics, heat-transfer and chemical-reaction processes. *A Lecture Course*, **HTS/80/1**, Imperial College, London, 1980.

- [19] Patankar, S.V., *Numerical heat transfer and fluid flow*. McGraw-Hill, New York, 197 pp, 1980.
- [20] Gaskell, P.H. and Lau, A.K.C., Curvature-compensated convective transport: SMART, a new boundedness-preserving transport algorithm, *International Journal for Numerical Methods in Fluids*, **8**, 617-641, 1988.
- [21] Brookes, A.N. and Hughes, T.J.R., Streamline upwind/Petrov Galerkin formulations for convection dominated flows with particular emphasis on the Navier-Stokes equations. *Computer Methods in Applied Mechanics and Engineering*, **32**, 199-259, 1982.
- [22] Marchuk, G.I., *Methods of Numerical Mathematics*. Springer-Verlag, New York, 102 pp, 1975.
- [23] Hervouet, J.-M. and Jankowski, J., Comparing numerical simulations of free surface flows using non-hydrostatic Navier–Stokes and Boussinesq equations. *Proceedings of the 4th International Conference Hydroinformatics*. 23-27 July 2000, Iowa, USA, 2000.
- [24] Ferguson, R. I., Parsons, D.R., Lane, S.N. and Hardy, R.J., Flow in meander bends with recirculation at the inner bank. *Water Resources Research*, **39**, ESG 2-1 – 2-13, 2003.
- [25] Rameshwaran, P. and Shiono, K., Computer modelling of two-stage meandering channel flows. *Proceedings of the Institution of Civil Engineers- Water & Maritime Engineering*, **156**, 326-339, 2003.
- [26] Morvan, H., Knight D., Wright, N, Tang X. and Crossley A. (2008) The concept of roughness in fluvial hydraulics and its formulation in 1D, 2D and 3D numerical simulation models. *Journal of Hydraulic Research*, **46**, 191-208.
- [27] Meselhe, E.A. and Sotiropoulos, F., Three-dimensional numerical model for open-channels with free-surface variation. *Journal of Hydraulic Research*, **38**, 115-121, 2000.
- [28] Morvan, H., Pender, G., Wright, N.G., and Ervine, D.A., Three-dimensional hydrodynamics of meandering compound channels. *Journal of Hydraulic Engineering*, **128**, 674-682, 2002.
- [29] Malcherek, A., Application of TELEMAC-2D in a narrow estuarine tributary, *Hydrological Processes*, **14**, 2293-2300, 2000.

**Figure Captions**

**Figure 1** UK Flood Channel Facility (FCF)

**Figure 2** Channel geometry

**Figure 3** Meshes

**Figure 4** Comparison of the flow variable between meshes (PHOENICS)

**Figure 5** Comparison of streamwise velocity in the main channel (MC1-MC11) along with regression parameters. Solid line shows 1:1 agreement; dashed line is linear regression line fitted by least squares.

**Figure 6** Comparison of streamwise velocity on the floodplain (FP1-FP9) along with regression parameters. Solid line shows 1:1 agreement; dashed line is linear regression line fitted by least squares.

**Figure 7** Comparison of streamwise velocity

**Figure 8** Comparison of transverse velocity in the main channel (MC1-MC11) along with regression parameters. Solid line shows 1:1 agreement; dashed line is linear regression line fitted by least squares.

**Figure 9** Comparison of transverse velocity on the floodplain (FP1-FP9) along with regression parameters. Solid line shows 1:1 agreement; dashed line is linear regression line fitted by least squares.

**Figure 10** Comparison of secondary vectors at apex cross-section MC3.

**Figure 11** Comparison of turbulent kinetic energy (TKE) in the main channel (MC1-MC11) along with regression parameters. Solid line shows 1:1 agreement; dashed line is linear regression line fitted by least squares.

**Figure 12** Comparison of turbulent kinetic energy (TKE) on the floodplain (FP1-FP9) along with regression parameters. Solid line shows 1:1 agreement; dashed line is linear regression line fitted by least squares.

**Figure 13** Comparison of turbulent kinetic energy (TKE).

**Figure 14** Comparison of bed shear stress at whole apex section.

**Figure 15** Comparison of free surface elevation along with regression parameters. Solid line shows 1:1 agreement; dashed line is linear regression line fitted by least squares.

**Figure 16** Frequency and Cumulative percentage distributions of model uncertainty including table of percentage data points with model uncertainty less than 10%, 25% and 50% of 90% variation in the whole field.

**Figure 17** Frequency and Cumulative percentage distributions of model error including table of percentage data points with model error less than 10%, 25% and 50% of 90% variation in the whole data field.

**Table Captions**

**Table 1.** Geometric parameters and flow condition

**Table 2.** Boundary conditions

**Table 3.** Roughness parameter function  $E$

**Table 4.** Summary of meshes

**Table 5.** Numerical details

**Table 6.** Roughness value  $k_s$

**Table 7.** Median values of Grid Convergence Index (GCI)

ACCEPTED MANUSCRIPT

**Table 1.** Geometric parameters and flow condition

Sinuosity	Cross-over angle	Meander belt width (m)	Floodplain width (m)	Wavelength (m)	Radius of Curvature (m)
1.374	60°	6.107	10.000	12.000	2.743
Floodplain longitudinal slope	Main channel top width (m)	Main channel side slope	Main channel depth (m)	Water depth (m)	Discharge (m <sup>3</sup> s <sup>-1</sup> )
0.996×10 <sup>-3</sup>	1.200	45°	0.150	0.200	0.250

**Table 2.** Boundary conditions

Code	Inlet	Outlet	Bottom channel boundary	Water surface
PHOENICS	Initially mean streamwise velocity and subsequent runs, fully developed flow conditions	Pressure at the outlet on the free surface $p = 0$ and fully developed flow condition $\partial U_i / \partial m = \partial k / \partial m = \partial \varepsilon / \partial m = 0$	Wall-function (Table 3) and local turbulence equilibrium $k = U_*^2 / \sqrt{c_\mu}$ and $\varepsilon = U_*^3 / \kappa Y$	Velocity normal to the free surface $W = 0$ and normal gradients of $U$ , $V$ , $k$ and $\varepsilon$ set to zero. Subsequent runs with water surface treatment
SSIIM	Initially logarithmic profile of velocities and subsequent runs, fully developed flow conditions	Pressure at the outlet on the free surface $p = 0$ and fully developed flow condition $\partial U_i / \partial m = \partial k / \partial m = \partial \varepsilon / \partial m = 0$	Wall-function (Table 3) and local turbulence equilibrium $k = U_*^2 / \sqrt{c_\mu}$ and $\varepsilon = U_*^3 / \kappa Y$	Velocity normal to the free surface $W = 0$ and normal gradients of $U$ , $V$ , $k$ and $\varepsilon$ set to zero
FLUENT	Initially mean streamwise velocity and subsequent runs, fully developed flow conditions	Pressure at the outlet on the free surface $p = 0$ and fully developed flow condition $\partial U_i / \partial m = \partial k / \partial m = \partial \varepsilon / \partial m = 0$	Wall-function (Table 3) and local turbulence equilibrium $k = U_*^2 / \sqrt{c_\mu}$ and $\varepsilon = U_*^3 / \kappa Y$	Velocity normal to the free surface $W = 0$ and normal gradients of $U$ , $V$ , $k$ and $\varepsilon$ set to zero
TELEMAC-3D	Mean streamwise velocity	Free surface elevation and fully developed flow condition $\partial U_i / \partial m = \partial k / \partial m = \partial \varepsilon / \partial m = 0$	Wall-function (Table 3) and local turbulence equilibrium $k = U_*^2 / \sqrt{c_\mu}$ and $\varepsilon = U_*^3 / \kappa Y$	Velocity normal to the free surface $W = 0$ and normal gradients of $U$ , $V$ , $k$ and $\varepsilon$ set to zero

**Table 3.** Roughness parameter function  $E$ 

Code	$E$
PHOENICS	$E = \begin{cases} 8.6 & Re_* < 3.7 \\ f(Re_*) & 3.7 \leq Re_* \leq 100. \\ 29.7/Re_* & Re_* > 100 \end{cases}$
SSIIM	$E = 30.0/Re_*$
FLUENT	$E = E' \exp[-\kappa \Delta B]$ where $E' = 9.8$ , $\Delta B = \begin{cases} 0 & Re_* < 2.25 \\ \left[ (1/\kappa) \ln \left( \frac{Re_* - 2.25}{87.75} \right) + C_{ks} Re_* \right] \sin[0.4258(\ln Re_* - 0.811)] & 2.25 \leq Re_* \leq 90 \\ (1/\kappa) \ln(1 + C_{ks} Re_*) & Re_* > 90 \end{cases}$ and $C_{ks} = 0.5$
TELEMAC-3D	$E = 30.0/Re_*$

**Table 4.** Summary of meshes

Code	Total number of cells	Number of downstream cells	Number of cross-stream cells	Number of vertical cells
PHOENICS, SSIIM, FLUENT	1408000	320	220	20
Code	Total number of 3D nodes	Number of 2D nodes	Number of 2D elements	Number of vertical planes
TELEMAC-3D	128178	7121	13984	18

**Table 5.** Numerical details

Code	Code type	Solution methods	Solution grid/point	Coupling with pressure/Solution technique	Convergence criteria
PHOENICS	Finite volume	Higher order SMART scheme	Non-Staggered	SIMPLEC	Mass balance within 0.1% and residuals reduced to 0.1%
SSIIM	Finite volume	Second order upwind scheme	Non-Staggered	SIMPLE	Mass balance within 0.1% and residuals reduced to 0.1%
FLUENT	Finite volume	Second order upwind scheme	Non-Staggered	SIMPLE	Mass balance within 0.1% and residuals reduced to 0.1%
TELEMAC-3D	Finite element	SUPG for velocities and water depth; Method of Characteristics for $k$ and $\epsilon$	Nodes	Fractional step method	Mass balance within 1% and termination tolerance for each variable between two time steps less than $10^{-4}$

**Table 6.** Roughness value  $k_s$ 

Code	$k_s$ (m)
PHOENICS	$5.50 \times 10^{-4}$
SSIIM	$2.00 \times 10^{-4}$
FLUENT	$2.00 \times 10^{-4}$
TELEMAC-3D	$4.50 \times 10^{-4}$

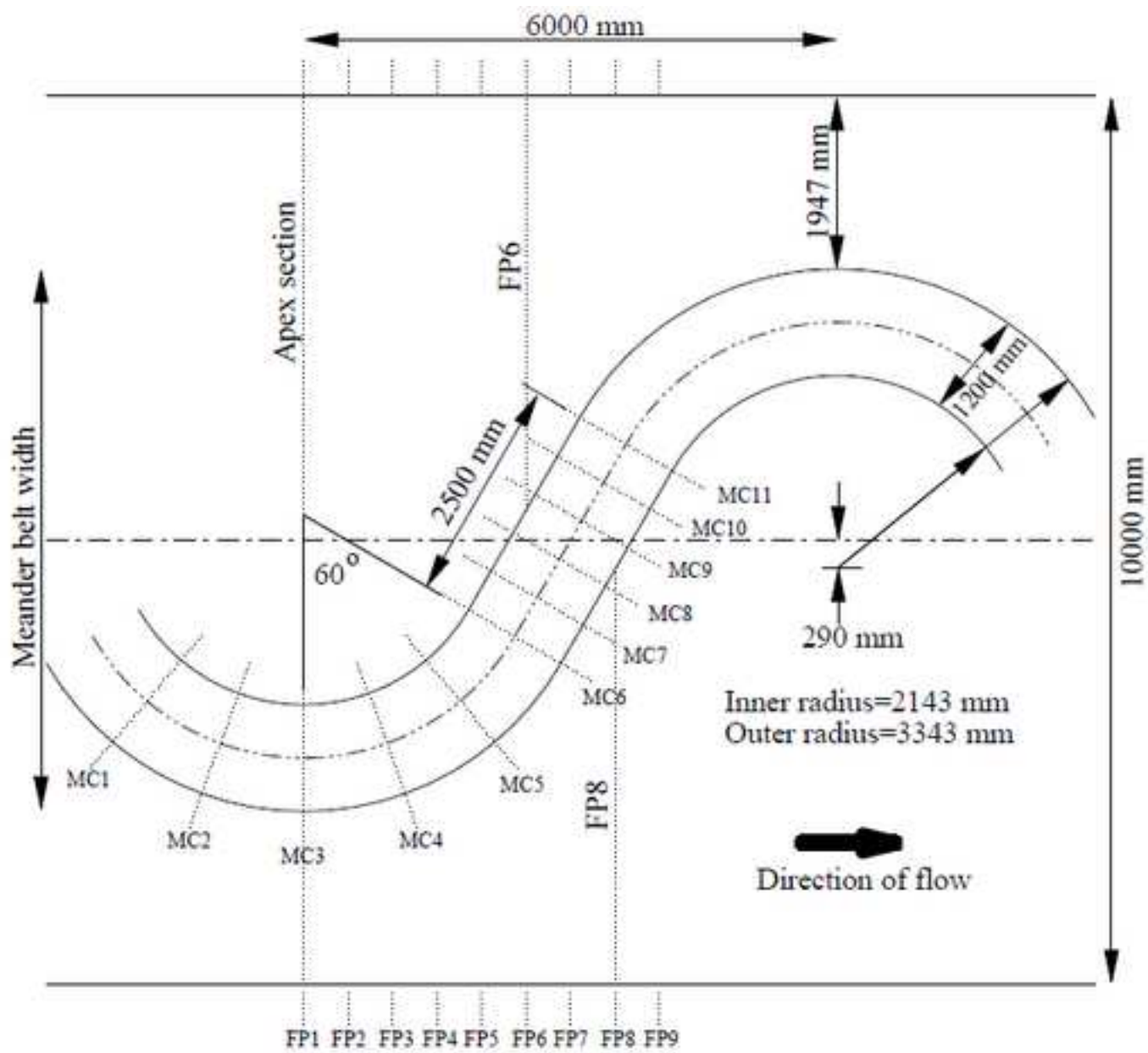
**Table 7.** Median values of Grid Convergence Index (GCI)

Meshes	$U_x$ (%)	$U_y$ (%)	$k$ (%)	Bed shear stress (%)
M1-M3	1.86	8.42	4.26	3.43
M2-M3	0.73	2.83	1.82	1.47

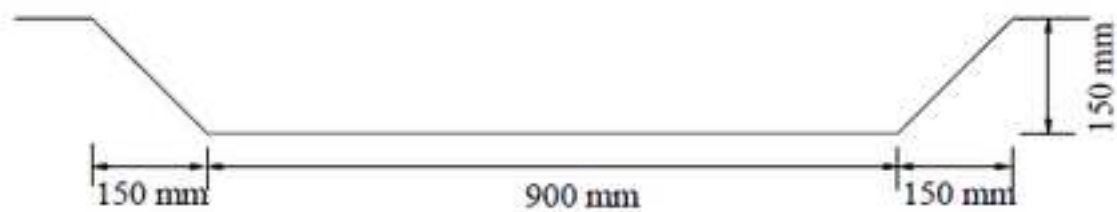
ACCEPTED MANUSCRIPT

Figure 01

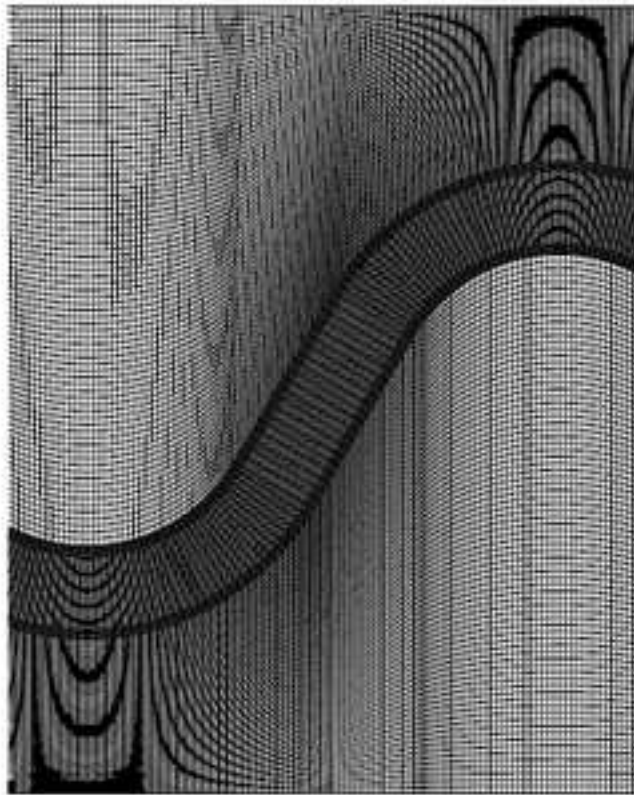




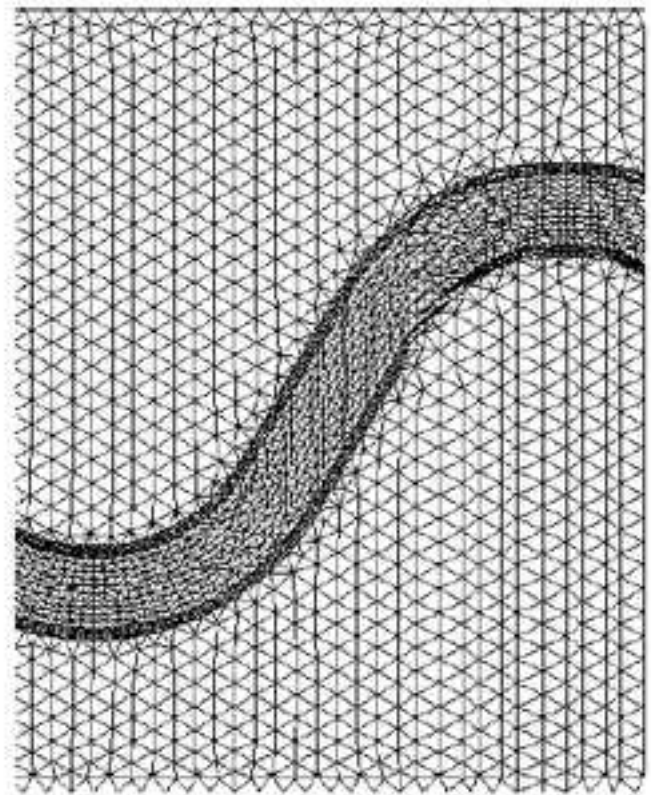
(a) Plan details



(b) Cross-section

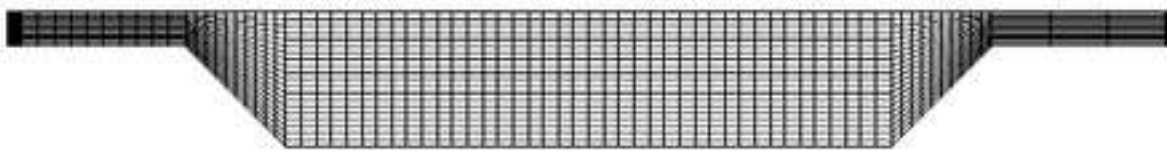


PHOENICS, SSIIM and FLUENT

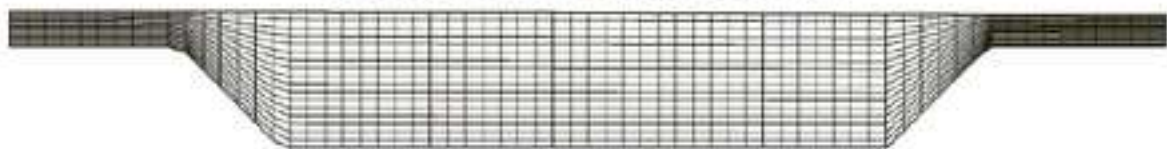


TELEMAC-3D

(a) Top plan view of the meshes

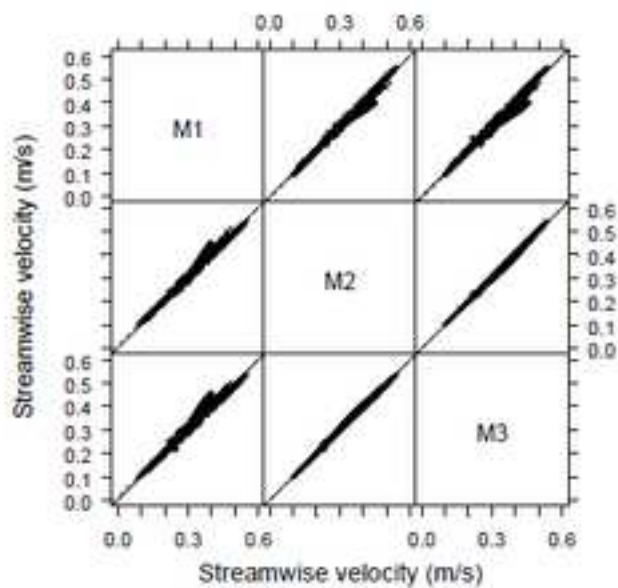


PHOENICS, SSIIM and FLUENT



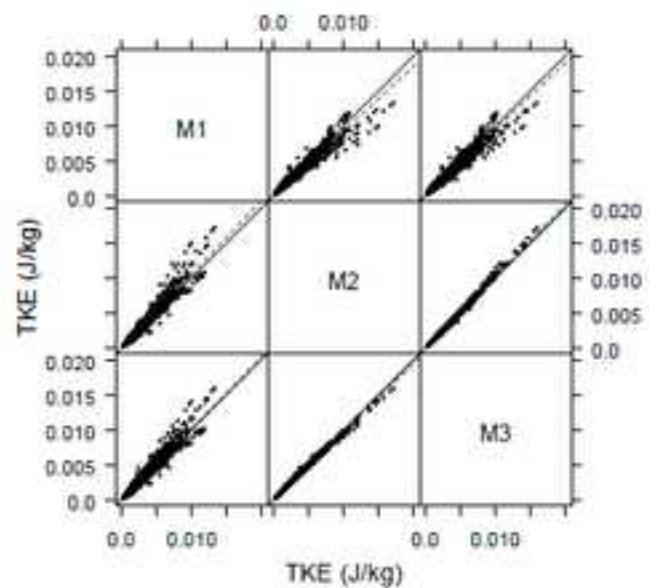
TELEMAC-3D

(b) Bend apex cross-sectional view of the main channel meshes



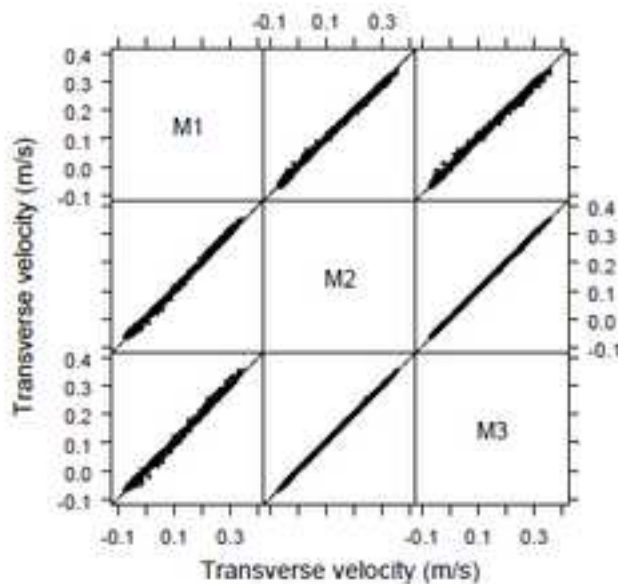
$R^2$	m	$c \times 10$	$R^2$	m	$c \times 10$	$R^2$	m	$c \times 10$
	M1		0.99	1.02	-0.10	0.98	1.01	-0.09
0.99	0.97	0.13		M2		1.00	1.00	0.00
0.98	0.97	0.16	1.00	0.99	0.02		M3	

(a) Streamwise velocity



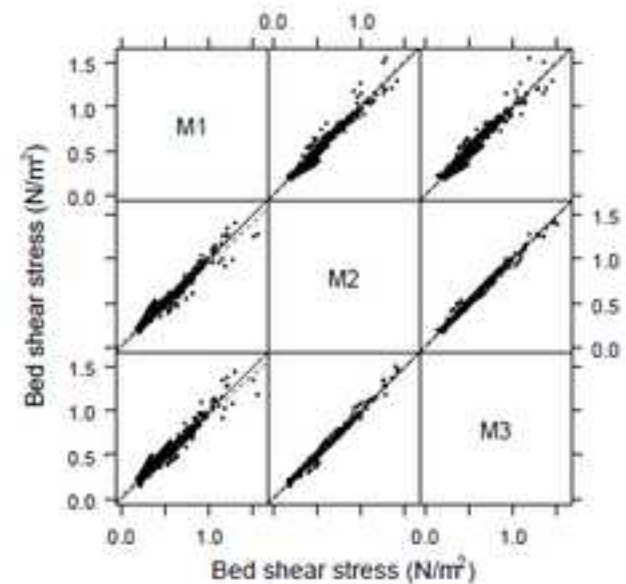
$R^2$	m	$c \times 10^2$	$R^2$	m	$c \times 10^2$	$R^2$	m	$c \times 10^2$
	M1		0.97	92	0.01	0.97	0.95	0.01
0.97	1.05	0.00		M2		1.00	1.03	0.00
0.97	1.02	0.00	1.00	0.97	0.00		M3	

(c) Turbulent kinetic energy (TKE)



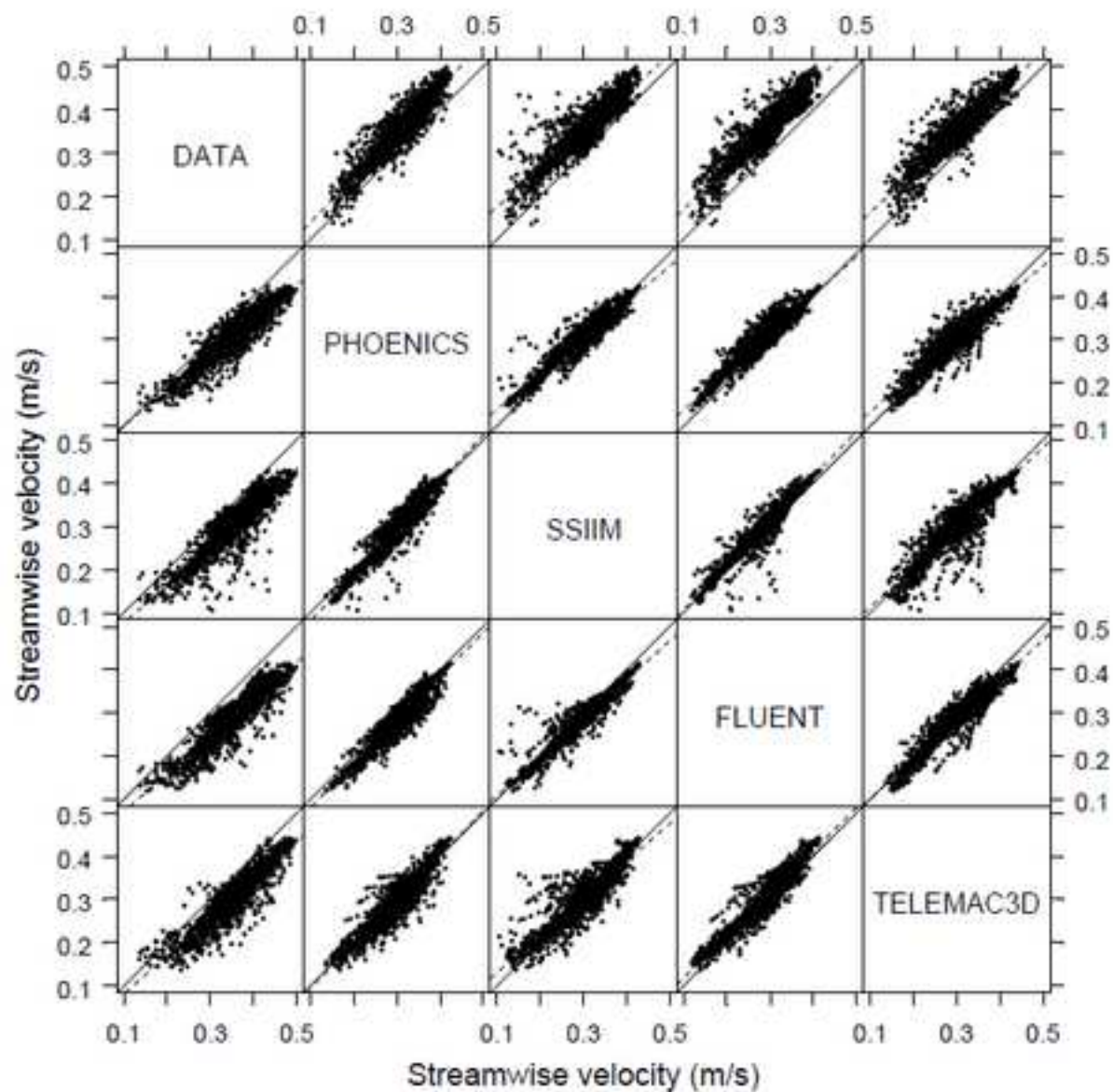
$R^2$	m	$c \times 10$	$R^2$	m	$c \times 10$	$R^2$	m	$c \times 10$
	M1		1.00	0.98	0.00	1.00	0.98	0.00
1.00	1.02	0.00		M2		1.00	1.00	0.00
1.00	1.02	0.00	1.00	1.00	0.00		M3	

(b) Transverse velocity

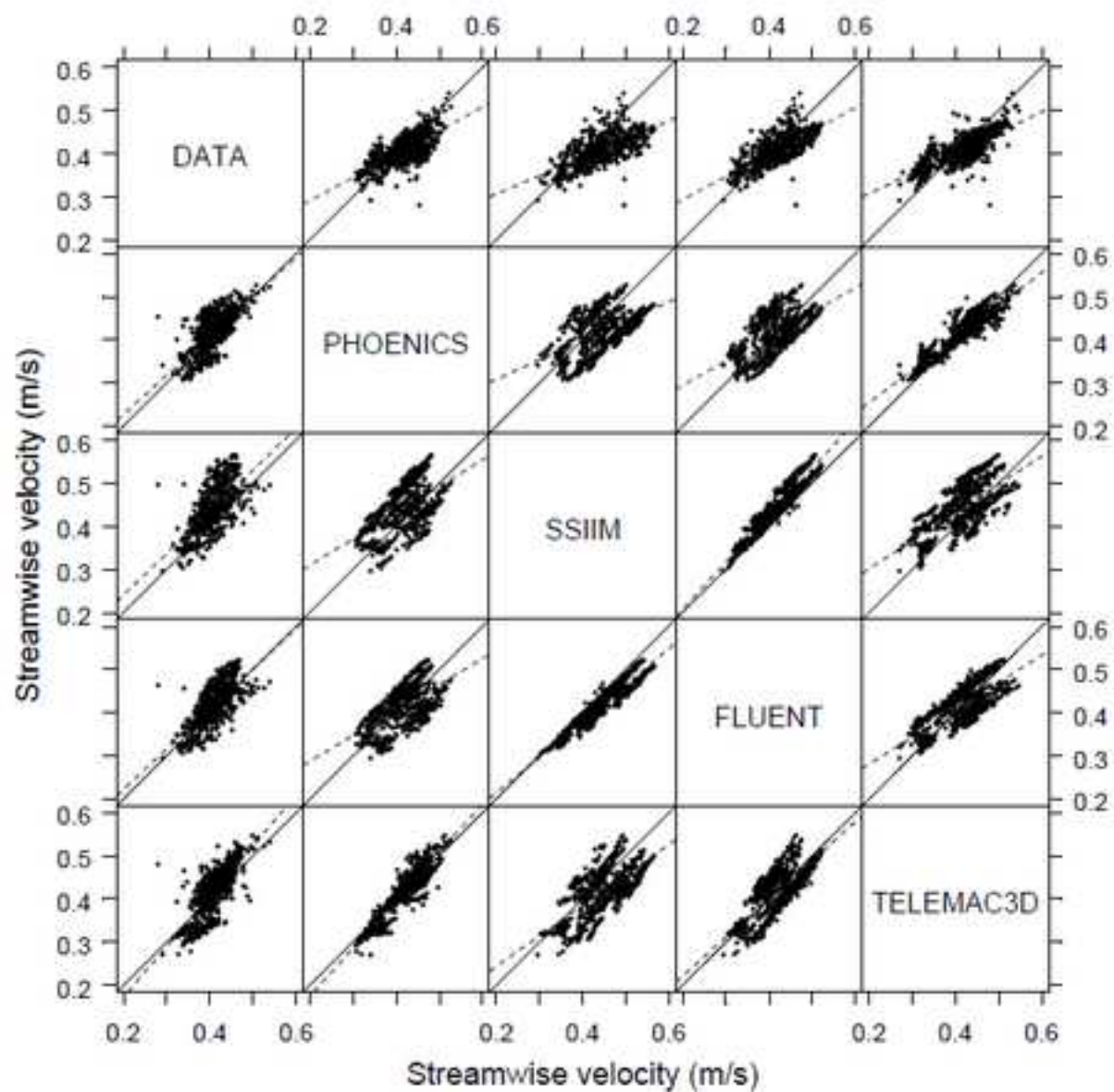


$R^2$	m	$c \times 10$	$R^2$	m	$c \times 10$	$R^2$	m	$c \times 10$
	M1		0.94	1.04	-0.17	0.93	1.02	-0.11
0.94	0.91	0.40		M2		0.99	0.99	0.06
0.93	0.91	0.42	0.99	1.00	0.01		M3	

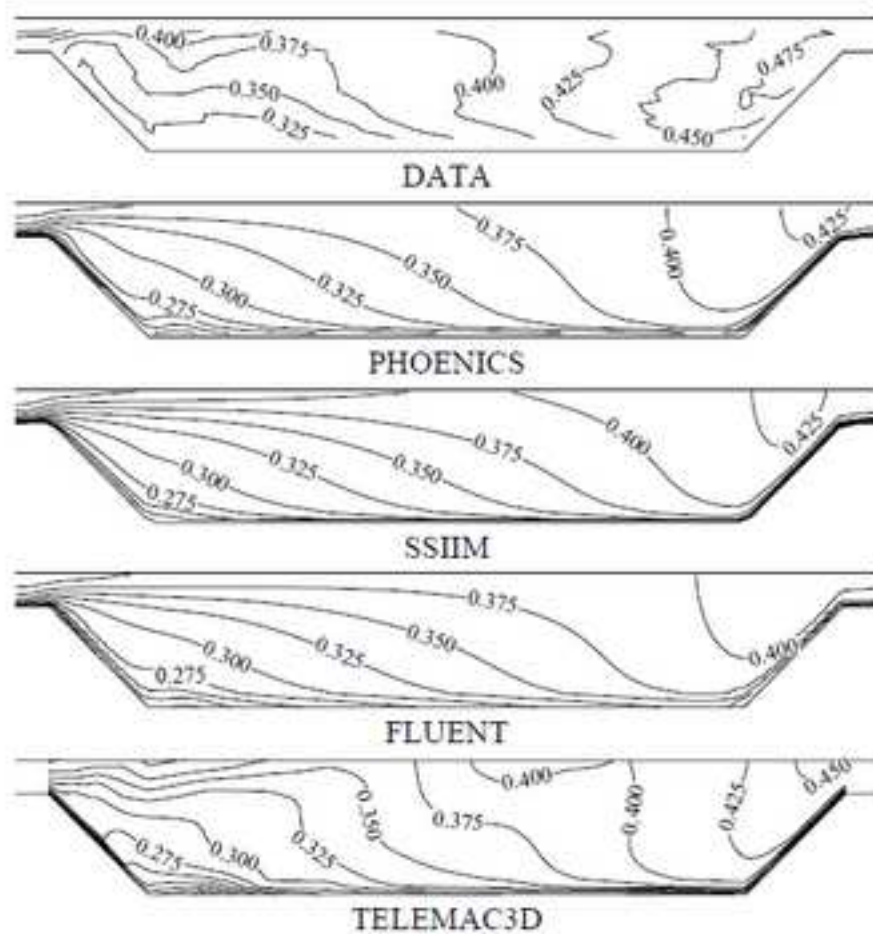
(d) Bed shear stress



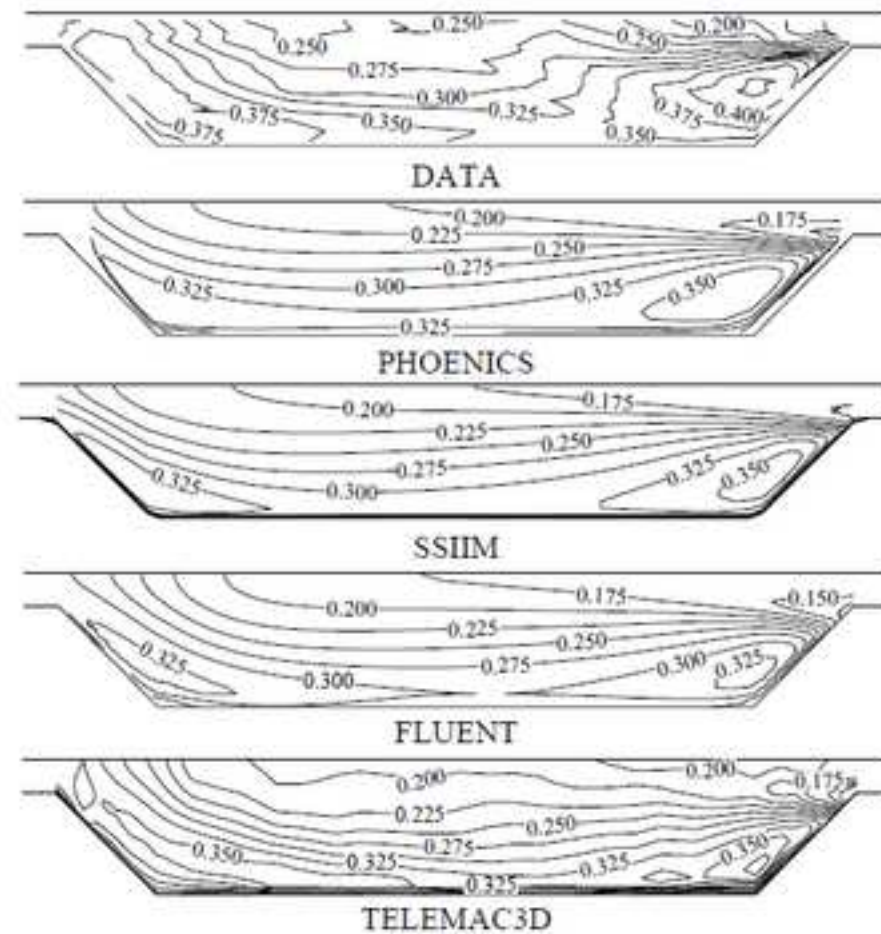
$R^2$	m	c	$R^2$	m	c	$R^2$	m	c	$R^2$	m	c	$R^2$	m	c	
	DATA			0.84	1.04	0.04	0.79	0.88	0.09	0.84	0.97	0.07	0.82	0.93	0.07
0.84	0.81	0.02	PHOENICS			0.89	0.83	0.06	0.90	0.89	0.05	0.87	0.84	0.05	
0.79	0.89	-0.01	0.89	1.08	-0.03	SSIIM			0.92	1.03	0.01	0.79	0.92	0.02	
0.84	0.86	-0.01	0.90	1.01	-0.02	0.92	0.90	0.02	FLUENT			0.90	0.92	0.01	
0.82	0.88	-0.01	0.87	1.03	-0.01	0.79	0.86	0.04	0.90	0.98	0.02	TELEMAC3D			



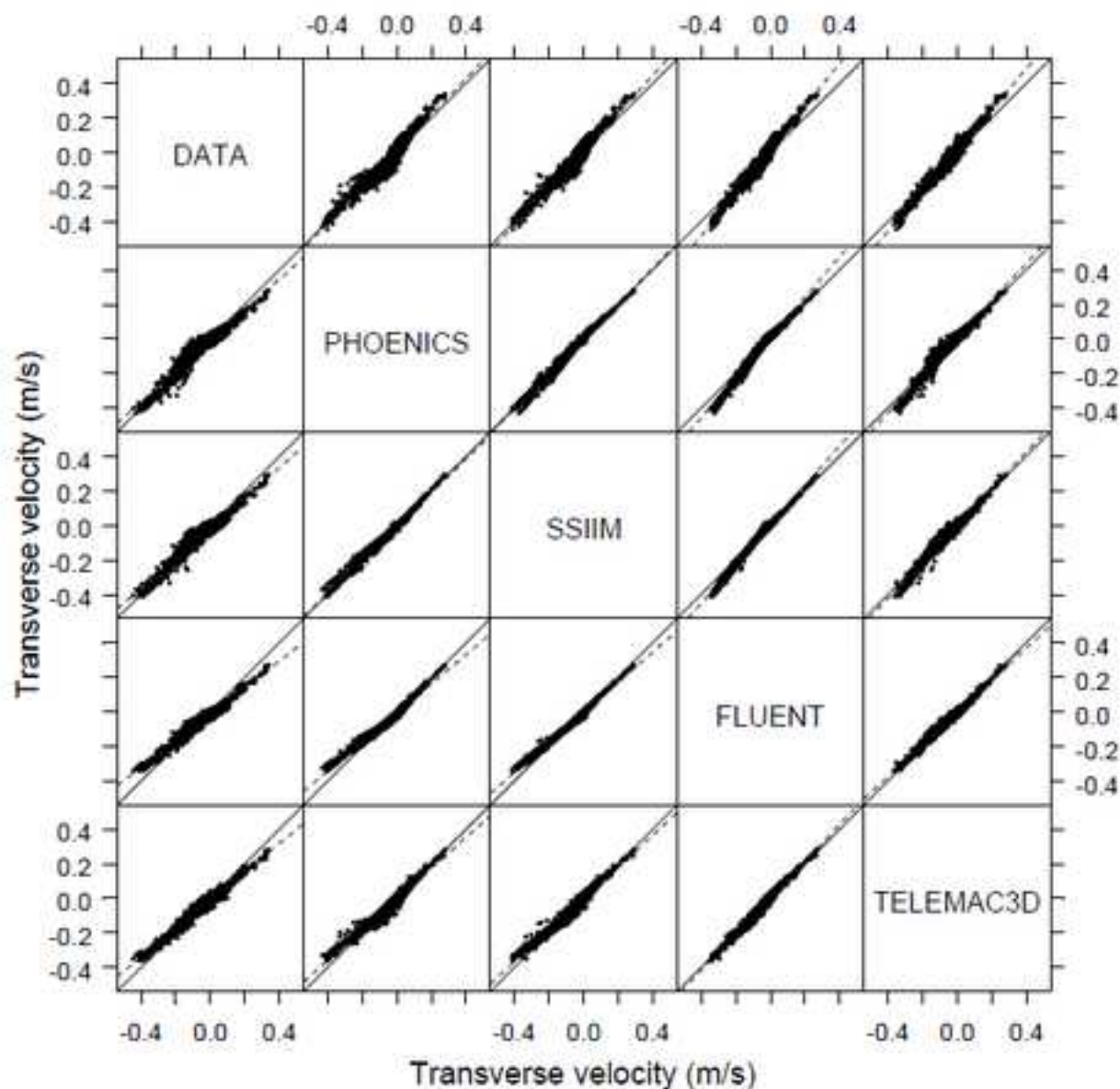
$R^2$	m	c	$R^2$	m	c	$R^2$	m	c	$R^2$	m	c	$R^2$	m	c
	DATA		0.49	0.54	0.18	0.41	0.43	0.22	0.49	0.53	0.19	0.55	0.47	0.21
0.49	0.91	0.05	PHOENICS			0.27	0.45	0.22	0.34	0.57	0.18	0.84	0.75	0.10
0.41	0.97	0.05	0.27	0.61	0.19	SSIIM			0.91	1.09	-0.01	0.46	0.65	0.17
0.49	0.93	0.04	0.34	0.59	0.17	0.91	0.83	0.05	FLUENT			0.56	0.63	0.15
0.55	1.17	-0.06	0.84	1.11	-0.05	0.46	0.71	0.10	0.56	0.89	0.04	TELEMAC3D		



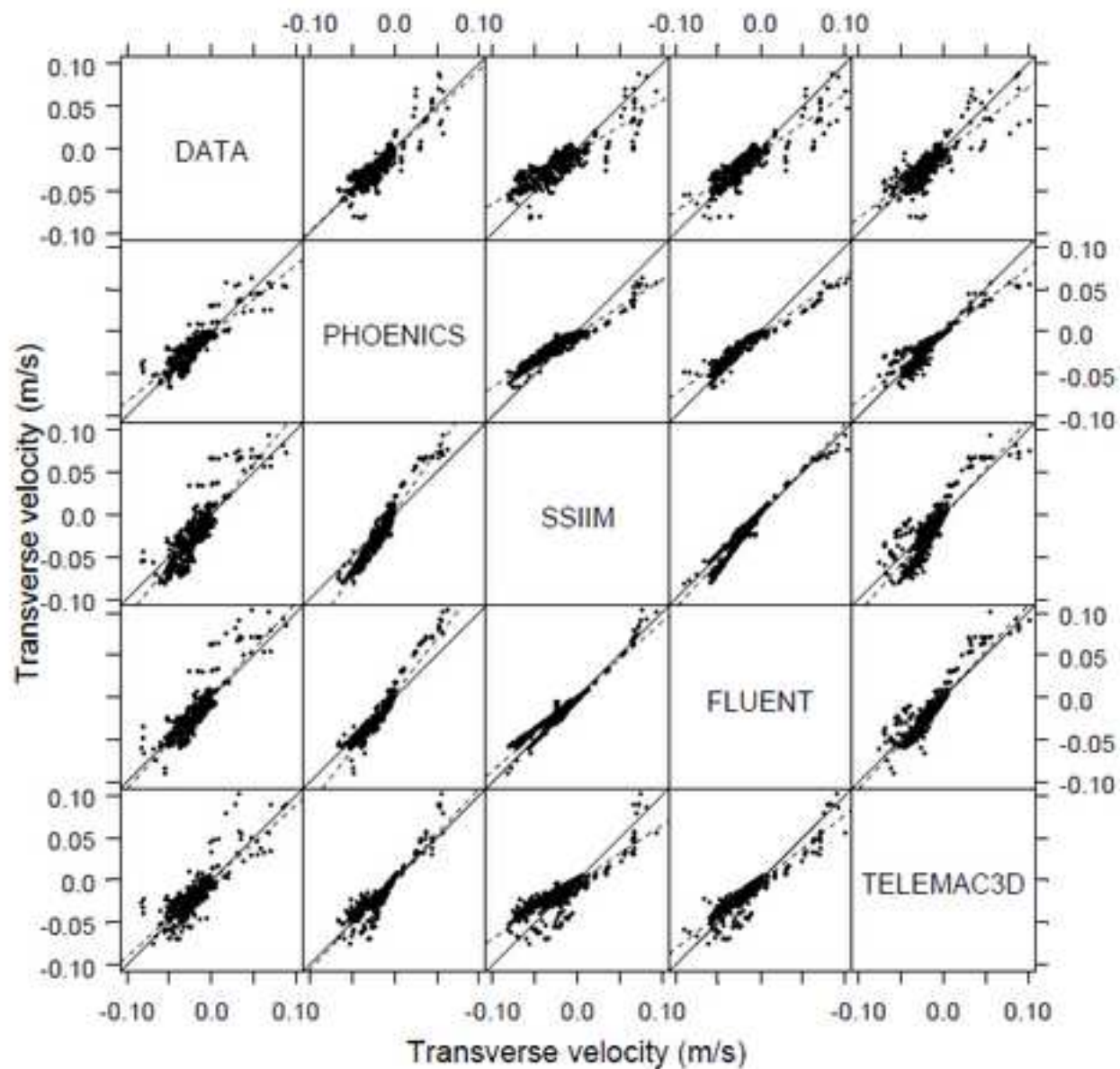
(a) Apex cross-section MC3



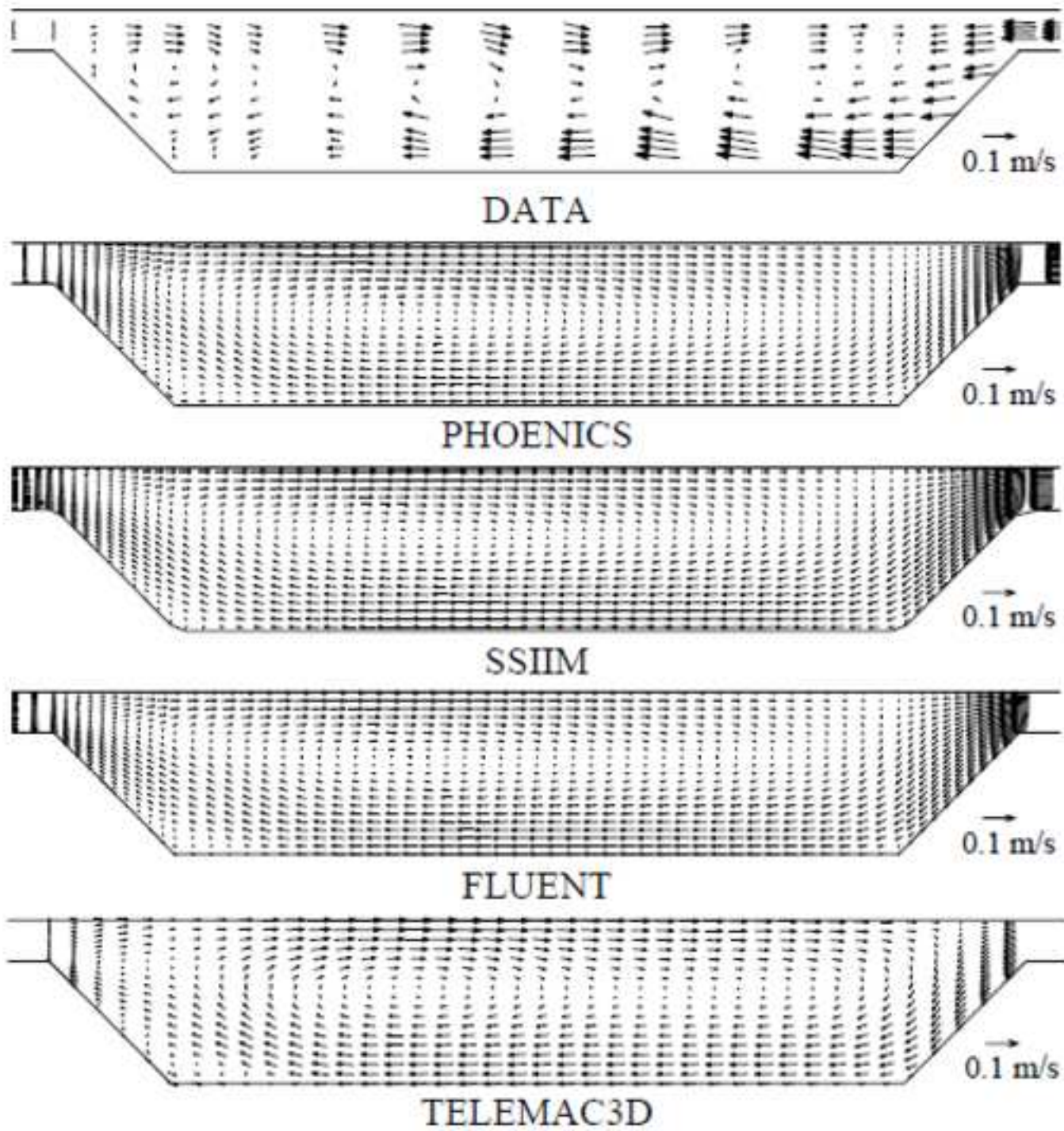
(b) Crossover cross-section MC8

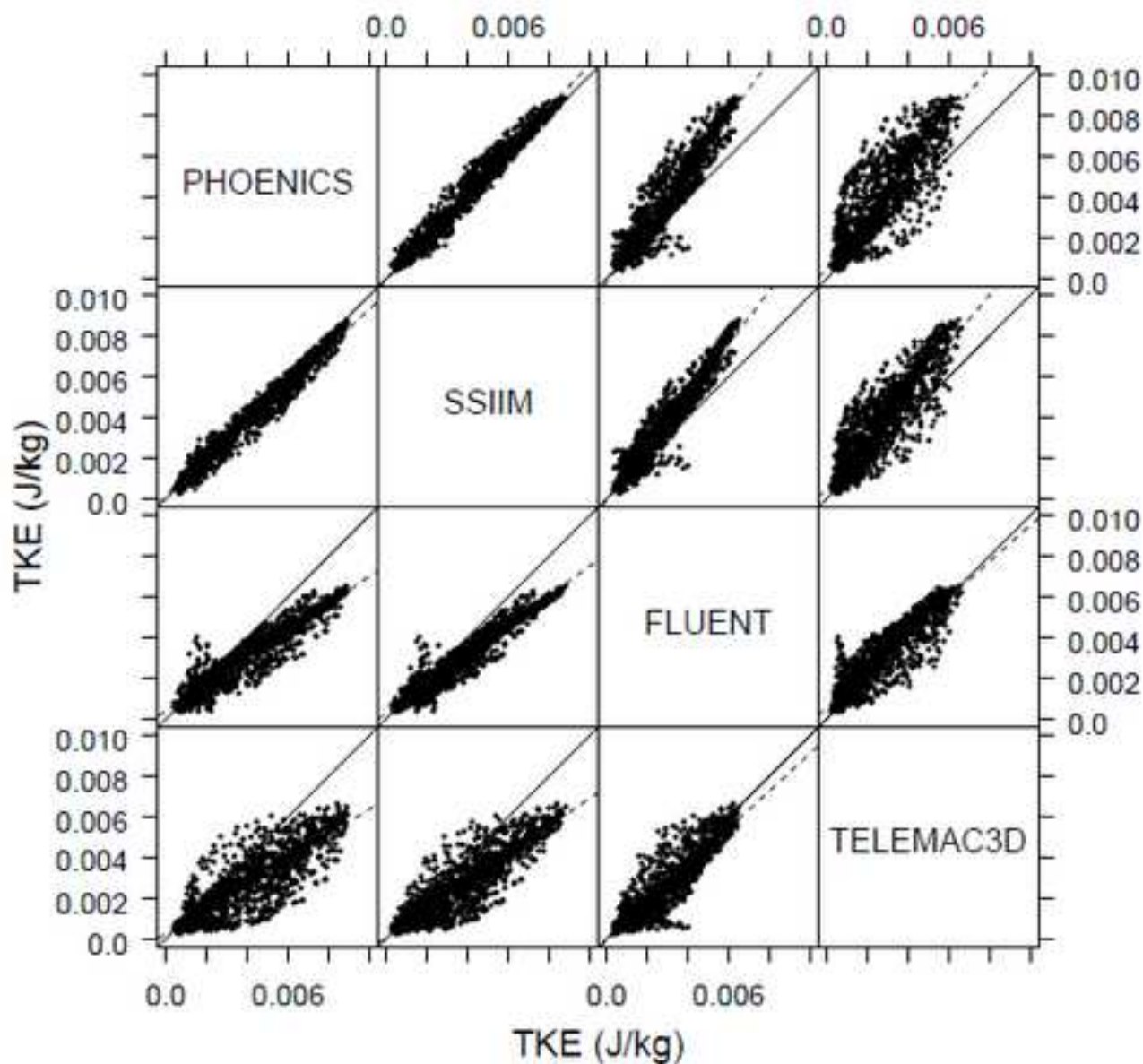


$R^2$	m	$c \times 10$	$R^2$	m	$c \times 10$	$R^2$	m	$c \times 10$	$R^2$	m	$c \times 10$	$R^2$	m	$c \times 10$	
	DATA			0.93	1.05	0.07	0.94	1.08	0.10	0.96	1.25	0.14	0.97	1.18	0.11
0.93	0.89	-0.01	PHOENICS			0.99	1.02	0.03	0.98	1.16	0.05	0.96	1.08	0.02	
0.94	0.87	-0.12	0.99	0.97	-0.04	SSIIM			0.99	1.14	0.02	0.97	1.06	-0.01	
0.96	0.77	-0.12	0.98	0.84	-0.05	0.99	0.87	-0.02	FLUENT			0.98	0.93	-0.03	
0.97	0.82	-0.11	0.96	0.89	-0.04	0.97	0.92	-0.01	0.98	1.06	0.02	TELEMAC3D			

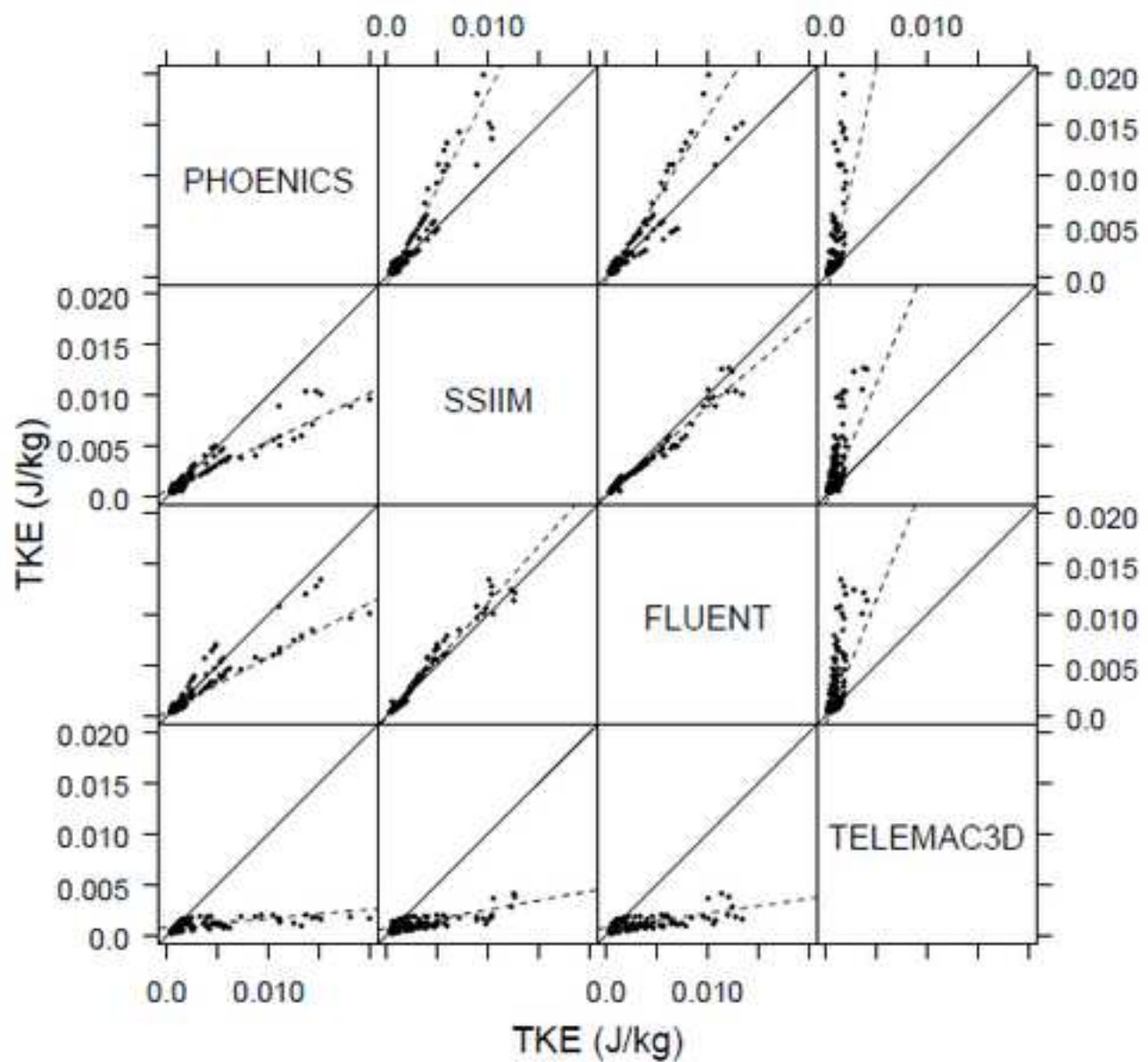


$R^2$	m	$c \times 10$	$R^2$	m	$c \times 10$	$R^2$	m	$c \times 10$	$R^2$	m	$c \times 10$	$R^2$	m	$c \times 10$
DATA			0.77	0.95	-0.02	0.73	0.61	-0.04	0.76	0.69	-0.05	0.69	0.77	-0.05
0.77	0.81	-0.02	PHOENICS			0.93	0.63	-0.02	0.92	0.70	-0.04	0.84	0.78	-0.04
0.73	1.20	-0.01	0.93	1.47	0.02	SSIIM			0.95	1.09	-0.02	0.76	1.13	-0.04
0.76	1.10	0.01	0.92	1.31	0.03	0.95	0.88	0.01	FLUENT			0.85	1.08	0.00
0.69	0.89	-0.01	0.84	1.07	0.01	0.76	0.67	-0.02	0.85	0.79	-0.02	TELEMAC3D		

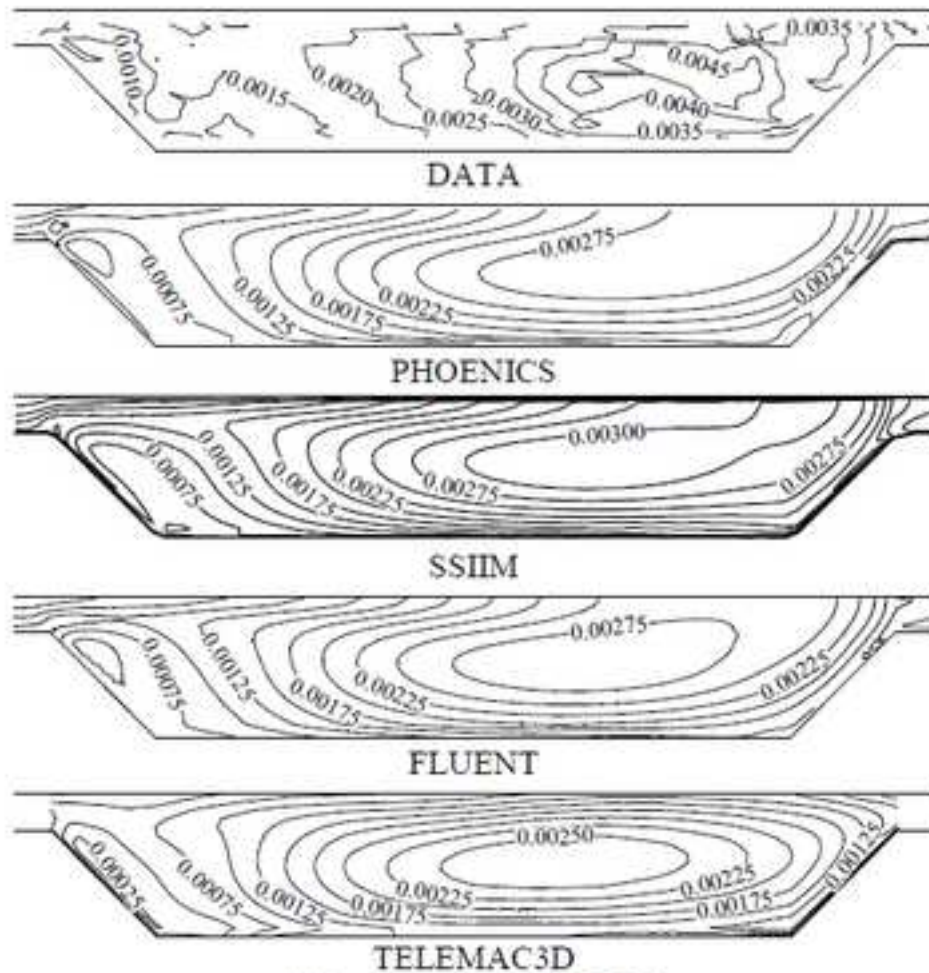




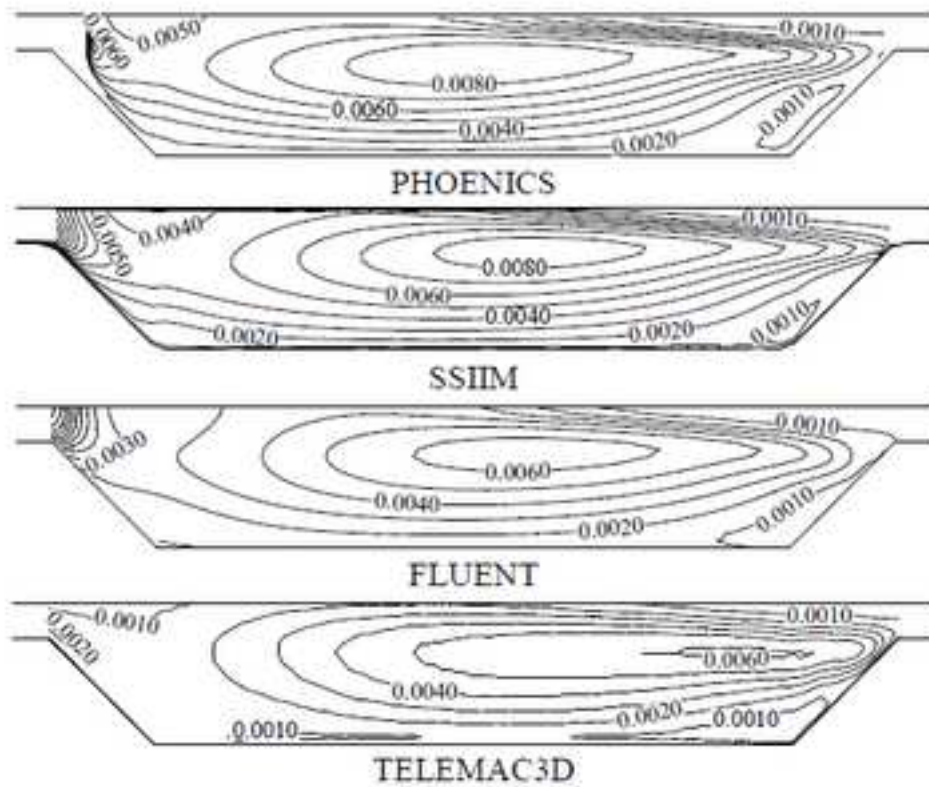
$R^2$	m	$c \times 10^2$	$R^2$	m	c	$R^2$	m	$c \times 10^2$	$R^2$	m	$c \times 10^2$
PHOENICS			0.97	1.06	-0.01	0.90	1.36	-0.02	0.75	1.23	0.05
0.97	0.92	0.02	SSIIM			0.93	1.29	-0.01	0.81	1.18	0.05
0.90	0.66	0.04	0.93	0.72	0.03	FLUENT			0.83	0.90	0.06
0.75	0.61	0.03	0.81	0.68	0.01	0.83	0.92	-0.01	TELEMAC3D		



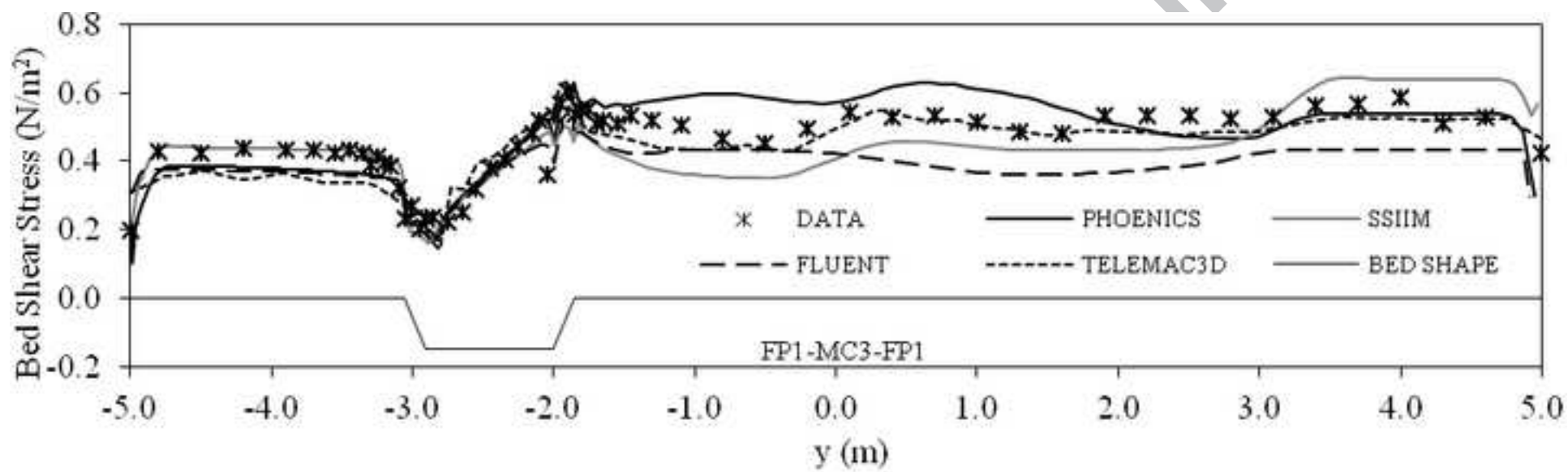
$R^2$	m	$c \times 10^2$	$R^2$	m	c	$R^2$	m	$c \times 10^2$	$R^2$	m	$c \times 10^2$
PHOENICS			0.92	1.91	-0.09	0.87	1.62	-0.05	0.41	4.60	-0.25
0.92	0.48	0.05	SSIIM			0.97	0.86	0.02	0.44	2.37	-0.08
0.87	0.54	0.04	0.97	1.13	-0.02	FLUENT			0.35	2.45	-0.09
0.41	0.09	0.07	0.44	0.18	0.07	0.35	0.15	0.07	TELEMAC3D		

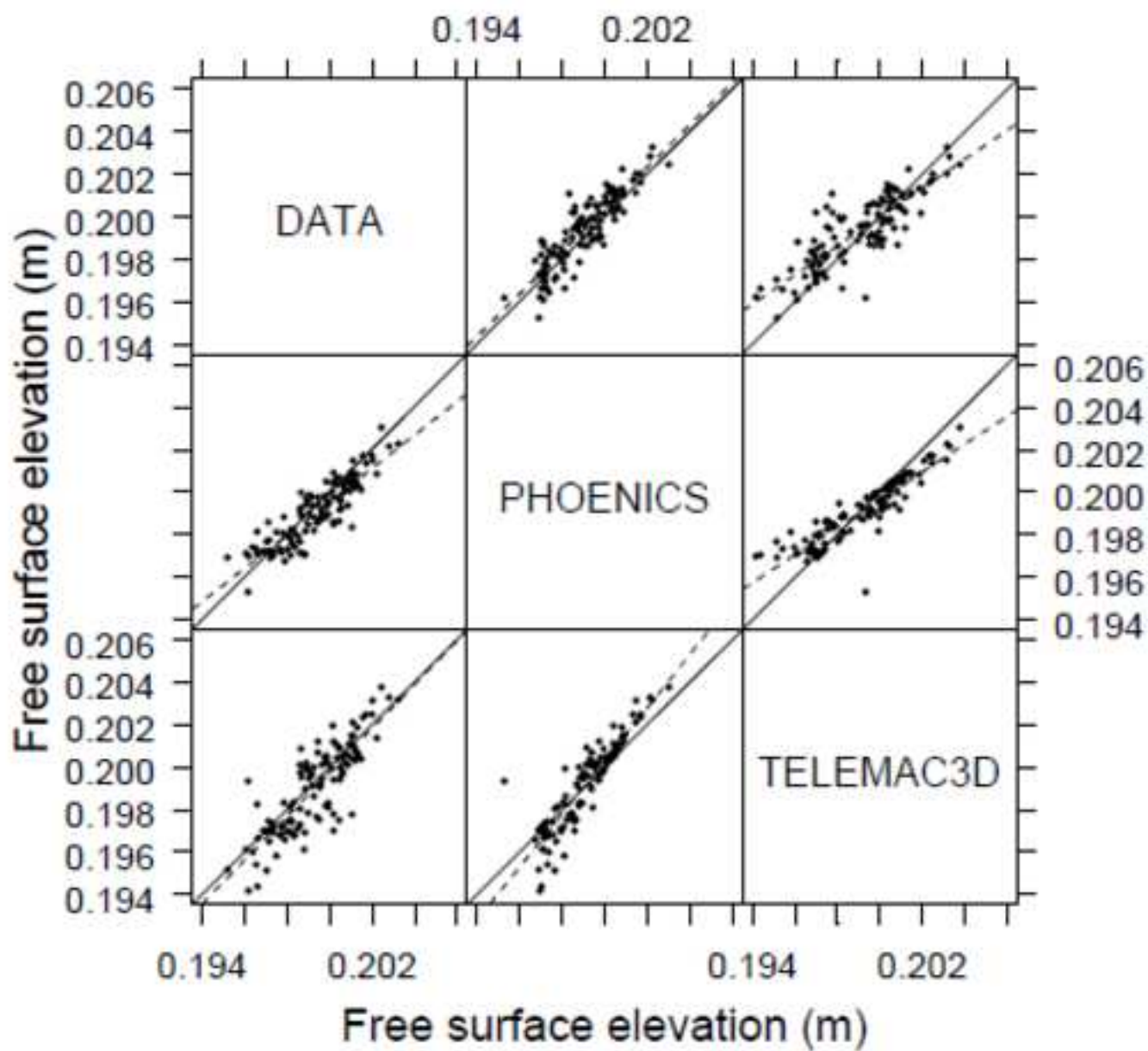


(a) Apex cross-section MC3

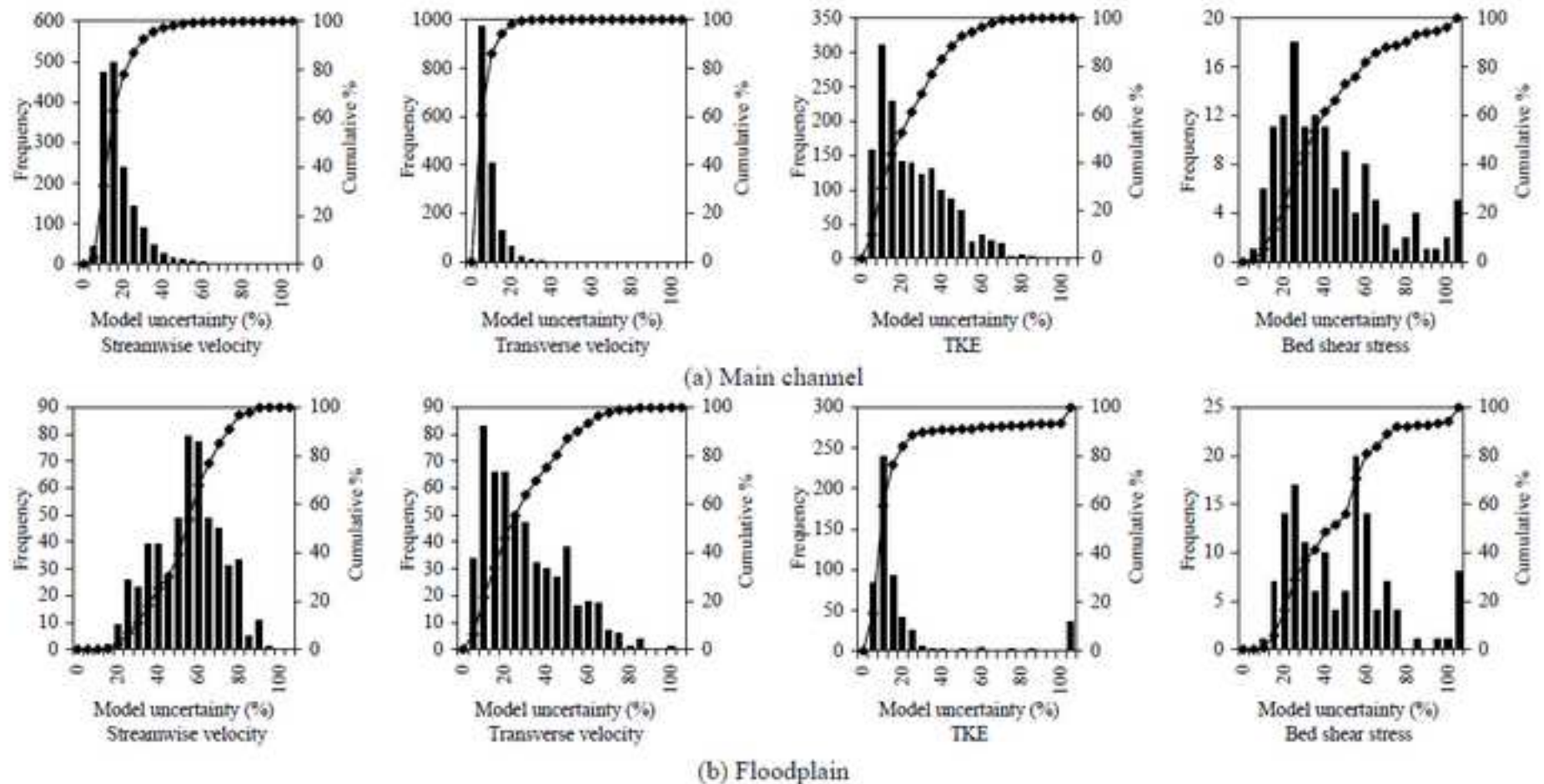


(b) Crossover section MC8

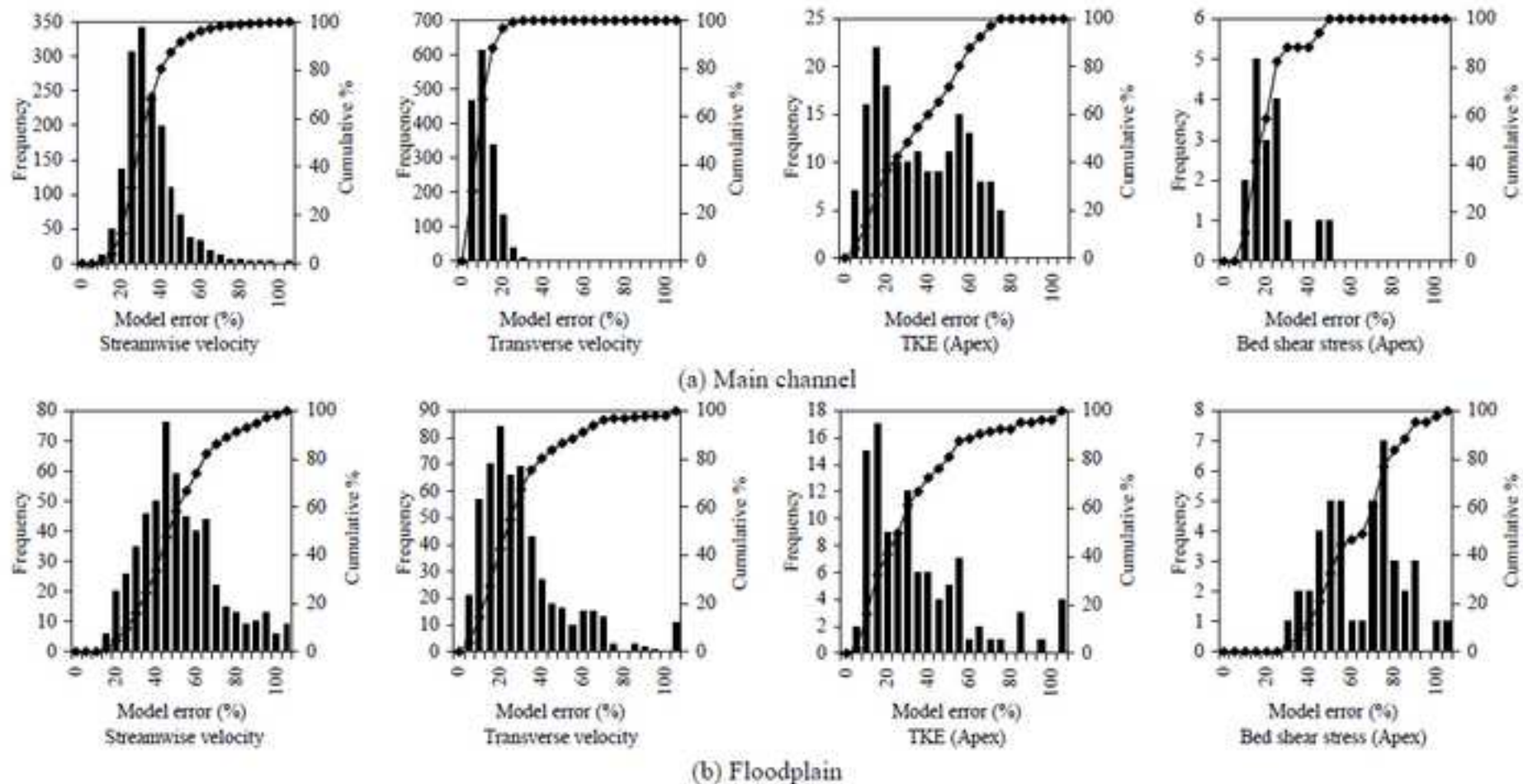




$R^2$	m	$c \times 10$	$R^2$	m	$c \times 10$	$R^2$	m	$c \times 10$
	DATA		0.78	0.99	0.02	0.70	0.68	0.63
0.78	0.78	0.43	PHOENICS			0.82	0.65	0.69
0.70	1.03	-0.06	0.82	1.25	-0.50	TELEMAC3D		



Flow variable	Main channel uncertainty					Floodplain uncertainty				
	No. of points	90% variation	<10%	<25%	<50%	No. of points	90% variation	<10%	<25%	<50%
Streamwise velocity	1606	0.2129 (Data)	32%	87%	99%	544	0.1188 (Data)	0%	7%	39%
Transverse velocity	1606	0.3875 (Data)	86%	99%	100%	544	0.0549 (Data)	22%	55%	87%
TKE	1606	0.0059 (Model)	29%	61%	93%	544	0.0029 (Model)	60%	89%	91%
Bed shear stress	133	0.3777 (Model)	5%	36%	73%	136	0.3441 (Model)	1%	29%	56%



Flow variable	Main channel error					Floodplain error				
	No. of points	90% variation	<10%	<25%	<50%	No. of points	90% variation	<10%	<25%	<50%
Streamwise velocity	1606	0.2129 (Data)	1%	32%	92%	544	0.1188 (Data)	0%	10%	59%
Transverse velocity	1606	0.3875 (Data)	67%	99%	100%	544	0.0549 (Data)	15%	55%	87%
TKE (Apex section only)	172	0.0036 (Data)	13%	42%	72%	105	0.0012 (Data)	16%	50%	81%
Bed shear stress (Apex section only)	17	0.3603 (Data)	12%	82%	100%	43	0.1761 (Data)	0%	0%	33%

**Figure Captions****Figure 1** UK Flood Channel Facility (FCF)**Figure 2** Channel geometry**Figure 3** Meshes**Figure 4** Comparison of the flow variable between meshes (PHOENICS)**Figure 5** Comparison of streamwise velocity in the main channel (MC1-MC11) along with regression parameters. Solid line shows 1:1 agreement; dashed line is linear regression line fitted by least squares.**Figure 6** Comparison of streamwise velocity on the floodplain (FP1-FP9) along with regression parameters. Solid line shows 1:1 agreement; dashed line is linear regression line fitted by least squares.**Figure 7** Comparison of streamwise velocity**Figure 8** Comparison of transverse velocity in the main channel (MC1-MC11) along with regression parameters. Solid line shows 1:1 agreement; dashed line is linear regression line fitted by least squares.**Figure 9** Comparison of transverse velocity on the floodplain (FP1-FP9) along with regression parameters. Solid line shows 1:1 agreement; dashed line is linear regression line fitted by least squares.**Figure 10** Comparison of secondary vectors at apex cross-section MC3.**Figure 11** Comparison of turbulent kinetic energy (TKE) in the main channel (MC1-MC11) along with regression parameters. Solid line shows 1:1 agreement; dashed line is linear regression line fitted by least squares.**Figure 12** Comparison of turbulent kinetic energy (TKE) on the floodplain (FP1-FP9) along with regression parameters. Solid line shows 1:1 agreement; dashed line is linear regression line fitted by least squares.**Figure 13** Comparison of turbulent kinetic energy (TKE).**Figure 14** Comparison of bed shear stress at whole apex section.**Figure 15** Comparison of free surface elevation along with regression parameters. Solid line shows 1:1 agreement; dashed line is linear regression line fitted by least squares.**Figure 16** Frequency and Cumulative percentage distributions of model uncertainty including table of percentage data points with model uncertainty less than 10%, 25% and 50% of 90% variation in the whole field.**Figure 17** Frequency and Cumulative percentage distributions of model error including table of percentage data points with model error less than 10%, 25% and 50% of 90% variation in the whole data field.